Cellular/Molecular

# Corticotropin Releasing Factor Mediates $K_{Ca}3.1$ Inhibition, Hyperexcitability, and Seizures in Acquired Epilepsy

**Manindra Nath Tiwari,[1] Sandesh Mohan,[1] Yoav Biala,[1] Oded Shor,[2,4] ⬤Felix Benninger,[2,3,4] and Yoel Yaari[1]**

[1]Department of Medical Neurobiology, Institute for Medical Research Israel-Canada, Hebrew University-Hadassah School of Medicine, Jerusalem, Israel 9112102, [2]Felsenstein Medical Research Center, Beilinson Hospital, Petach Tikva, Israel 4941492, [3]Department of Neurology, Rabin Medical Center, Petach Tikva, Israel 49141492, and [4]Sackler Faculty of Medicine, Tel Aviv University, Tel Aviv, Israel 6997801

Temporal lobe epilepsy (TLE), the most common focal seizure disorder in adults, can be instigated in experimental animals by convulsant-induced status epilepticus (SE). Principal hippocampal neurons from SE-experienced epileptic male rats (post-SE neurons) display markedly augmented spike output compared with neurons from nonepileptic animals (non-SE neurons). This enhanced firing results from a cAMP-dependent protein kinase A-mediated inhibition of $K_{Ca}3.1$, a subclass of $Ca^{2+}$-gated $K^+$ channels generating the slow afterhyperpolarizing $Ca^{2+}$-gated $K^+$ current ($I_{sAHP}$). The inhibition of $K_{Ca}3.1$ in post-SE neurons leads to a marked reduction in amplitude of the $I_{sAHP}$ that evolves during repetitive firing, as well as in amplitude of the associated $Ca^{2+}$-dependent component of the slow afterhyperpolarization potential ($K_{Ca}$-sAHP). Here we show that $K_{Ca}3.1$ inhibition in post-SE neurons is induced by corticotropin releasing factor (CRF) through its Type 1 receptor ($CRF_1R$). Acute application of $CRF_1R$ antagonists restores $K_{Ca}3.1$ activity in post-SE neurons, normalizing $K_{Ca}$-sAHP/$I_{sAHP}$ amplitudes and neuronal spike output, without affecting these variables in non-SE neurons. Moreover, pharmacological antagonism of $CRF_1Rs$ *in vivo* reduces the frequency of spontaneous recurrent seizures in post-SE chronically epileptic rats. These findings may provide a new vista for treating TLE.

*Key words:* channelopathy; CRF; hippocampus; intrinsic excitability; $K_{Ca}3.1$; temporal lobe epilepsy

---

**Significance Statement**

Epilepsy, a common neurologic disorder, often develops following a brain insult. Identifying key cellular mechanisms underlying acquired epilepsy is critical for developing effective antiepileptic therapies. In an experimental model of acquired epilepsy, principal hippocampal neurons manifest hyperexcitability because of downregulation of $K_{Ca}3.1$, a subtype of $Ca^{2+}$-gated $K^+$ ion channels. We show that $K_{Ca}3.1$ downregulation is mediated by corticotropin releasing factor (CRF) acting through its Type 1 receptor ($CRF_1R$). Congruently, acute application of selective $CRF_1R$ antagonists restores $K_{Ca}3.1$ channel activity, leading to normalization of neuronal excitability. In the same model, injection of a $CRF_1R$ antagonist to epileptic animals markedly decreases the frequency of electrographic seizures. Therefore, targeting $CRF_1Rs$ may provide a new strategy in the treatment of acquired epilepsy.

---

## Introduction

Temporal lobe epilepsy (TLE) is the most common form of adult epilepsy (Téllez-Zenteno and Hernández-Ronquillo, 2012). It is often instigated by a brain insult, triggering a cascade of structural and functional alterations, termed epileptogenesis, leading to the emergence of spontaneous recurrent seizures (SRSs)

(Becker, 2018). The mechanisms underlying epileptogenesis and sustaining ictogenesis are not well understood. Therefore, existing medication lacks specificity and provides only partial symptomatic relief while often causing adverse side effects. Moreover, ~30% of TLE patients become refractory to existing drugs (Kwan et al., 2011). It is therefore critical to identify new drug targets and develop target-directed medication for impeding epileptogenesis and for suppressing ictogenesis in TLE patients (Wahab, 2010).

Using the well-known pilocarpine-induced status epilepticus (SE) rat model of acquired TLE (Raol and Brooks-Kayal, 2012), we have recently shown that epileptogenesis leads to a widespread increase in the intrinsic excitability of hippocampal pyramidal cells. The main cause of this increase is suppression of the slow afterhyperpolarization (sAHP) (Tamir et al., 2017; Tiwari et al., 2019). In ordinary neurons, the sAHP that follows a

spike train comprises two partially overlapping components. One component arises from the activation of $K_{Ca}3.1$, a subtype of $Ca^{2+}$-gated $K^+$ ($K_{Ca}$) ion channels, encoded by *KCNN4*, via spike $Ca^{2+}$ influx (the $K_{Ca}$-sAHP component). The second component results from the augmented activation of the $Na^+/K^+$ ATPase (NKA) by spike $Na^+$ influx (the NKA-sAHP component) (Gulledge et al., 2013; Tiwari et al., 2018; Sahu and Turner, 2021). Intriguingly, the sAHP suppression in epileptic (post-SE) CA1 pyramidal cells was because of a marked reduction of the $K_{Ca}$-sAHP component and its underlying current ($I_{sAHP}$), whereas the NKA-sAHP component was unchanged (Tiwari et al., 2019). Furthermore, $K_{Ca}$-sAHP/$I_{sAHP}$ suppression in post-SE neurons was mediated by protein kinase A (PKA), as acute application of PKA inhibitors reversed this suppression, while normalizing the intrinsic neuronal excitability of post-SE neurons (Tiwari et al., 2019). A positive association between PKA activity, intrinsic neuronal excitability, and ictogenesis in experimental and human TLE has been suggested in a recent study (Zhang et al., 2021).

Here we sought to identify the signaling pathway that causes sustained PKA hyperactivity in post-SE neurons. Multiple neurotransmitters were shown to activate PKA in CA1 pyramidal cells, leading to $K_{Ca}$-sAHP/$I_{sAHP}$ suppression (Madison and Nicoll, 1986; Pedarzani and Storm, 1993; Haug and Storm, 2000). One of these neurotransmitters, corticotropin releasing factor (CRF), has been implicated in the pathogenesis of human epilepsy (Brunson et al., 2001; Yang et al., 2017) and can induce convulsive seizures when injected intracerebroventricularly into rodent brains (Ehlers et al., 1983; Baram and Schultz, 1991). Furthermore, CRF is stored and released by a subpopulation of hippocampal interneurons that innervate CRF receptors-expressing pyramidal cells (Chen et al., 2004; Gunn et al., 2019).

Based on these previous studies, we have hypothesized that augmented CRF/PKA signaling causes $K_{Ca}$-sAHP/$I_{sAHP}$ downregulation and intrinsic hyperexcitability in post-SE CA1 pyramidal cells. The results of our present study support this working hypothesis and implicate CRF Type 1 receptor ($CRF_1R$) in this cascade. Moreover, they show that intercepting $CRF_1R$/PKA signaling can impede ictogenesis in acquired TLE *in vivo*.

## Materials and Methods

*Ethical approval.* All experimental protocols were approved by the Animal Care and Use committees of the Hebrew University in Jerusalem and the Tel-Aviv University and Rabin Medical Center.

*Induction of SE.* We used the standard protocol to evoke epileptogenesis and chronic TLE in rats (Turski et al., 1983; Sanabria et al., 2001; Tiwari et al., 2019). Male Wistar rats (150-175 g) were injected intraperitoneally with a single dose of pilocarpine (300-380 mg/kg), inducing SE in ~80% of the animals. Peripheral muscarinic effects were reduced by prior subcutaneous administration of methyl-scopolamine (1 mg/kg, s. c.). Diazepam (0.1 mg/kg) was administered intraperitoneally to seizing rats 2 h after SE onset, terminating convulsions. The 24 h mortality rate of pilocarpine-injected rats was ~10%. The surviving rats constituted the post-SE group. Rats receiving the same drug treatment protocol, but without pilocarpine (therefore not experiencing SE), constituted the non-SE control group.

*Preparation of hippocampal slices.* Using the standard procedure used in our laboratory (Sanabria et al., 2001; Tiwari et al., 2019), slices were prepared from 44 non-SE and 57 post-SE rats 5-6 weeks after drug treatment, at which time they weighed ~400 g. Slices were also prepared from 31 naive (not receiving any drug treatment) male Wistar rats (150-175 g). In brief, rats were decapitated under isoflurane anesthesia, and transverse dorsal hippocampal slices (400 μm) were prepared with a vibratome. The slices were transferred to a storage chamber perfused

with carboxygenated (95% $O_2$ and 5% $CO_2$) aCSF at room temperature. For recording, slices were placed one at a time in an interface chamber and superfused with warmed (35.0°C) carboxygenated aCSF containing blockers of synaptic transmission, as indicated.

*Solutions and chemicals.* The standard aCSF comprised the following (in mM): 124 NaCl, 3.5 KCl, 1 $MgCl_2$, 1.6 $CaCl_2$, 26 $NaHCO_3$, and 10 glucose (pH 7.35; osmolarity 305 mOsm). It also contained CNQX (15 μM), APV (50 μM), picrotoxin (100 μM), and 3-aminopropyl-diethoxymethyl-phosphinic acid hydrate (CGP-55845; 1 μM) to block glutamatergic and GABAergic synaptic transmission, as well as 50 μM ZD7288, a blocker of hyperpolarization-activated cyclic nucleotide-gated channels (used to prevent sAHP shunting) (Tiwari et al., 2018). The standard aCSF composition was modified in specific experiments as follows: the aCSFs designed to block voltage-gated $Ca^{2+}$ channels (Cd+Ni-aCSF) also contained $CdCl_2$ and $NiCl_2$ (200 μM each). The aCSFs used for evoking $Ca^{2+}$ spikes and $I_{sAHP}$s (TTX-aCSF) also contained 0.5 μM TTX, 5 mM 4-AP, 10 μM XE991, and 100 nM apamin. The latter two drugs were used to isolate the $I_{sAHP}$s by blocking conjointly activated $K_V7$/M and SK channels, respectively. In experiments using CRF or astressin, 10% BSA was added to the aCSFs (BSA-aCSF) to prevent peptide adhesion to the plastic tubing (Haug and Storm, 2000).

*Reagents.* Picrotoxin, CGP-55845, $NiCl_2$ $CdCl_2$, pilocarpine, scopolamine, BSA, NBI27914, and TRAM-34 were obtained from Sigma-Aldrich. CNQX, APV, and anti-$CRF_1R$ rabbit polyclonal antibody were purchased from Alomone Labs. ZD7288, CRF, antalarmin (ATM), and astressin 2B were obtained from Tocris Bioscience. Diazepam (Assival) was purchased from TEVA. H89 and anti-rabbit secondary antibody were procured from Abcam-Zotal. The rat CRF ELISA kit was procured from MyBioSource. Drugs were diluted 1:1000 when added to the aCSF from stock solutions.

*Electrophysiology.* Intracellular recordings were obtained using sharp glass microelectrodes containing 4 M $K^+$-acetate (90-110 MΩ) and a bridge amplifier (Axoclamp 2B, Molecular Devices) allowing switching between current-clamp and discontinuous voltage-clamp recordings (switching frequency between current injection and voltage sampling was 6-8 kHz). Signals were filtered on line at 1.5 kHz, digitized at a sampling rate of $\geq 10$ kHz, and stored by a personal computer using a data acquisition system (Digidata 1322A) and pCLAMP9 software (Molecular Devices).

Impalements into neurons was performed "blindly" in the stratum pyramidale of area CA1b, and neurons were identified as pyramidal cells according to their characteristic spike morphology and firing pattern (Azouz et al., 1994; Jensen et al., 1996). The pyramidal cells included in this study had a stable resting membrane potential ($V_m$) of at least −60 mV and an overshooting action potential. To reduce variations in spike output and in sAHP amplitudes across the pyramidal cells because of differences in resting $V_m$ (Tiwari et al., 2018), all current-clamp recordings were made from a "holding" $V_m$ of −70 mV maintained by constant current injection.

Two stimulation paradigms were used to evoke fast $Na^+$ spikes followed by dual-component sAHPs in standard aCSF. In one paradigm, spikes and sAHPs were evoked by 1-s-long depolarizing current pulses of increasing intensities (from 150 pA to 1.2 nA in 150 pA increments). In a second paradigm, a 3-s-long train of 150 spikes was generated by injecting brief (2-ms-long), suprathreshold depolarizing current pulses (3-4 nA) at 50 Hz. The size of a dual-component sAHP was assessed by measuring its amplitudes at two time points after stimulation offset, namely, at 1 and 7 s, yielding the amplitudes of the early-sAHP and late-sAHP, respectively. The "area under the curve" (or integral) of the sAHP provided another measure of its size (Tiwari et al., 2018, 2019). The second stimulation paradigm was used also to evoke "pure" NKA-sAHPs in slices perfused with Cd-Ni aCSF (Mohan et al., 2019, 2021). In both paradigms, the evoked sAHPs were stable over a period of at least 1 h.

To evoke "pure" $K_{Ca}$-sAHPs, slices were perfused in TTX aCSF. A series of 90-ms-long depolarizing current pulses were injected into neurons in steps of 100 pA until a $Ca^{2+}$ spike was generated (the rheobase current was usually between 400 and 500 pA), which was followed by a $K_{Ca}$-sAHP. The size of the latter potential was measured at its peak. In these same neurons, we also evoked $I_{sAHP}$s using discontinuous voltage-

clamp mode. From a holding $V_m$ of $-70$ mV, the voltage was stepped to $-15$ mV for 100 ms. This was followed by a slow outward current, which was measured at its peak amplitude (Tiwari et al., 2019). The recordings of both $K_{Ca}$-sAHPs and $I_{sAHP}$s were stable over a period of at least 1 h, contrasting the rundown of these signals within 10-20 min in patch-clamp recordings even at room temperature (Velumian et al., 1997; Haug and Storm, 2000). The amplitude of these responses was measured at their peaks.

*ELISA.* Expression of CRF protein was measured in hippocampal tissue of non-SE and post-SE rats using Rat CRF ELISA kit and following manufacturer's instructions (catalog #MBS269052) (Delawary et al., 2010; Fortes et al., 2017). Each rat provided two hippocampi, which were homogenized in 0.01 M PBS followed by centrifugation at 7500 rpm. Supernatant was collected and samples (diluted 1:1) were incubated in ELISA wells (precoated rat CRF monoclonal antibody) at 37°C for 90 min, followed by washing the ELISA plate with washing buffer (PBS). The detection antibody (biotin-labeled rat CRF polyclonal antibody) was then added to the ELISA plate wells after which they were incubated at 37°C for 60 min. After washing 3 times, the enzyme conjugate (Avidin-peroxidase) was added to the wells, which were then incubated at 37°C for 30 min. After washing 5 times, the color reagent solution was added to the wells, which were then incubated at 37°C for 30 min. Next, the color reagent C (tetramethyl-benzidine) was added to the wells and optical densities were recorded within 10 min at 450 nm by ELISA reader (ELx 800 Universal Microplate Reader BIO-TEK Instruments). The concentrations (pg/ml) of CRF were calculated using a standard curve.

*Western blotting.* CRF$_1$R protein expression analysis was performed in hippocampal tissues of non-SE and post-SE rats using Western blot technique according to standard protocol (Tiwari et al., 2010; Gai et al., 2016). Each rat provided two hippocampi, which were homogenized in ice-cold radio-immunoprecipitation assay buffer. Tissue homogenates were centrifuged at $15,000 \times g$ for 15 min at 4°C, and supernatants were collected. Protein concentration was determined using the Bradford method (Bio-Rad). The proteins were denatured in boiling water for 10 min and resolved on 10% SDS-PAGE. The proteins were then transferred to a nitrocellulose membrane, followed by blocking of nonspecific sites with 5% nonfat skimmed milk for 1 h at room temperature. The membrane was incubated with antibodies directed against CRF$_1$R (1:1000; catalog #ACR-050; Alomone Labs) and GAPDH (1:20,000; catalog #G8796; Sigma-Aldrich) proteins in 3% BSA for 12 h at 4°C, followed by repetitive washing with TBS. It was then incubated with HRP-conjugated secondary antibodies (1:5000 goat anti-rabbit and 1:20,000 goat anti-mouse) for 1 h at room temperature. After multiple washing, protein bands were developed by an enhanced chemiluminescence substrate under chemiluminescence gel doc system. The integrated band intensity was measured by ImageJ software (freely available on National Institutes of Health website), and data were presented as band intensity ratios (CRF$_1$R/GAPDH).

*Telemetric EEG recordings.* Recordings of the EEG of 13 post-SE rats were performed using the small animal telemetry system (Millar Instruments). To implant the EEG electrodes and transmitters, the rats were deeply anesthetized with ketamine (10 mg/kg; Vetoquinol) and xylazine (100 mg/kg; Eurovet). Transmitters were implanted into the right side of the abdominal cavity. Electrodes were then positioned at the stereotaxic coordinates $-1.5$ posterior, $\pm 1.5$ lateral relative to bregma in contact with the cerebral cortex and fixed using dental cement (Methylmethacrylate Resin, Unifast Trad). Following a recovery period of 24 h, EEG recordings were made with a sampling rate of 2 kHz.

Once stable EEG signals were obtained, monitoring was continuously performed for 48 h. After 24 h of recording, rats were randomly divided into two groups and injected with either vehicle (DMSO) or with 20 mg/kg ATM dissolved in DMSO. Detection of electrographic SRSs was performed using a customized software of the EEGgui MATLAB toolbox (Sick et al., 2013). In brief, each 1 h recording period was analyzed for seizure detection using short time period Fourier transformation. Average spectral power was measured for 24 h segments before and after injections. Power in the major frequency bands was calculated using short time period Fourier transformation for each 2 s period of EEG activity for the entire 48 h recording period. All power

measurements were normalized, and EEG epochs containing spike discharges were detected by first comparing power in each frequency band with the power observed in preinjected epochs. Significant change in power was defined if any frequency band exceeded that of the control EEG power by 4 SDs. Then, each EEG epoch was examined for a particular pattern of significant frequency changes that were unique to spike discharges. Comparisons of power changes in each frequency band with known spike discharges containing EEG records provided the pattern for detecting spike discharges in the EEG records. Further determination of electrographic SRSs in EEG records of all animals was performed without experimenter intervention.

*Data analyses.* GraphPad QuickCalcs, SPSS version 25 and MS Excel were used to perform the statistical analyses. Plots of number of spikes (Ns) versus stimulus intensity (I, in nA) were fitted with second-order polynomial regression equation: $f(y) = b_2 x^2 + b_1 x + b_0$. The initial slope of the regression line (parameter $b_1$) provided the slope (spike response gain) of the relationship (Tamir et al., 2017; Tiwari et al., 2019). Plots of sAHP amplitudes versus number of spikes were fitted with linear regression equation: $f(y) = ax + b$ (a, the slope of the regression line).

In pharmacological experiments, each neuron served as its own control (measurements were made in a single cell before and after drug application). Each slice was used for recording from one neuron only. Different slices from the same animal were used for different pharmacological experiments. A recording session lasted at least 15 min before drug application and over 30 min thereafter. Drug effects used for analyses were measured 30 min after drug application.

Statistical comparisons were made, as indicated, using two-tailed paired or unpaired Student's $t$ test, one- or two-tailed Wilcoxon signed rank test, one-way ANOVA, and one- or two-tailed Mann–Whitney tests. In the 18 comparisons using Student's $t$ test, the distributions of the control data groups (sample size varying between $n = 17$ and $n = 148$) was tested for departure from a normal distribution using a one-sample Kolmogorov–Smirnov test. In all cases, the exact (two-tailed) significance was $> 0.15$ (values ranged from 0.158 to 0.944).

Results are presented without normalization (unless stated otherwise), as mean $\pm$ SEM. In all statistical tests, minimal significance level was set to $p < 0.05$. Values of $n$ represent the number of neurons, unless stated differently.

*Data availability.* The data generated and analyzed in the current study are available from the corresponding author on reasonable request.

## Results

### CRF increases the excitability of CA1 pyramidal cells while suppressing the $K_{Ca}$-sAHP

In the first series of experiments, we tested the effects of CRF on the excitability of CA1 pyramidal cells in naive rats (young rats not subjected to any drug treatment; see Materials and Methods). Application of 250 nM CRF to slices in standard aCSF caused a mild ($\sim 6$ mV) but significant depolarization of resting $V_m$ (from $-67.4 \pm 0.6$ to $-61.6 \pm 2.1$ mV; $n = 9$; $t = 2.8$; df = 8; $p = 0.023$; paired Student's $t$ test), without affecting $R_N$ (from $76.0 \pm 9.0$ to $74.0 \pm 9.6$ MΩ; $n = 9$; $t = 0.37$; df = 8; $p = 0.72$; paired Student's $t$ test) or spike amplitude ($85.6 \pm 2.0$ to $89.1 \pm 2.4$ mV; $n = 9$; $t = 1.5$; df = 8; $p = 0.173$; paired Student's $t$ test).

Repetitive spike activity was elicited from a "holding" potential of $-70$ mV by 1-s-long depolarizing current pulses whose intensity (I) was increased from 150 pA to 1.2 nA in 150 pA increments. Suprathreshold current pulses evoked accommodating spike trains that were followed by sAHPs (Tiwari et al., 2019). The number of evoked spikes (Ns) and sAHP amplitudes increased with stimulus intensity. The firing response and sAHP evoked by a 0.3 nA pulse in a representative control neuron are shown in Figure 1A, B (Control).

Application of CRF markedly enhanced the firing of the pyramidal cells (Fig. 1A), while suppressing the sAHPs (Fig. 1B).
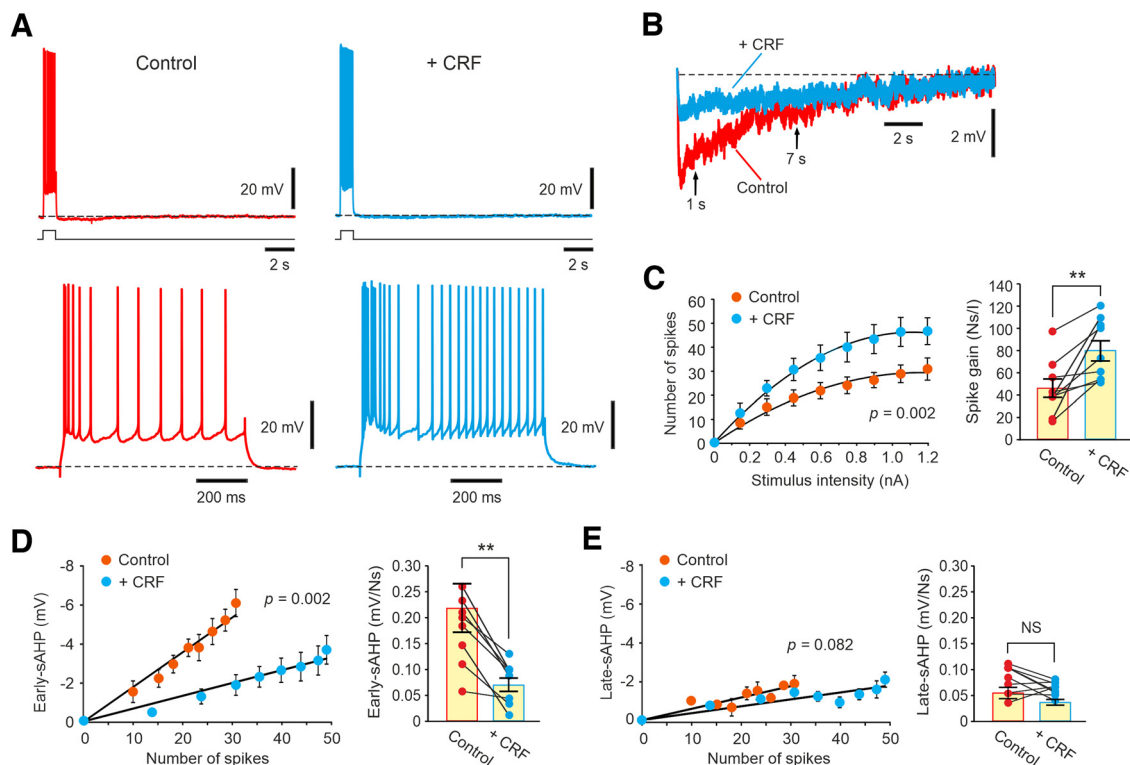
**Figure 1.** CRF increases spike output while suppressing the early-sAHP phase of the dual-component sAHP in ordinary CA1 pyramidal cells. *A*, Representative traces represent at two time scales the firing of a CA1 pyramidal cells stimulated by a 1-s-long depolarizing current pulses (0.3 nA) before (Control) and after application of 250 nM CRF (+ CRF). *B*, Overlaid enlarged traces of the sAHPs shown in *A*. Arrows indicate the time points used to measure the early- and slow-sAHP amplitudes (1 and 7 s after stimulus offset, respectively). *C*, The neurons were stimulated by a series of 1-s-long pulses, increasing in amplitudes (I) from 0 to 1.2 nA in steps of 150 pA. The summary plots depict the number of evoked spikes (Ns) as a function of stimulus intensity (I) before (Control) and after CRF application (+ CRF). Bar diagram represents the spike response gains (Ns/I) in the two conditions (n = 9). The gain is significantly increased by CRF. *D*, Same experiments as in *C*. Summary plots of early-sAHP amplitudes versus Ns. Bar diagram represents the early sAHP/Ns slopes before (Control) and after CRF application (+ CRF). The early-sAHP/Ns slope is significantly decreased by CRF. *E*, Same as in *D*, but the summary plot and bar diagram represent the late-sAHP amplitudes and late-sAHP/Ns slopes (n = 9). The late-sAHP/Ns slope is not affected by CRF. Data are mean ± SEM. **$p < 0.01$. NS, not significant.

The spike response gain (see Materials and Methods) increased to 174% of control value (from $46.1 \pm 8.2$ to $80.5 \pm 9.1$ Ns/I; $n = 9$; $p = 0.002$; one-tailed Wilcoxon signed rank test; Fig. 1C). We measured sAHP amplitudes at two time points after stimulus offset: 1 s (early-sAHP) and 7 s (late-sAHP; Fig. 1B; see Materials and Methods) (Tiwari et al., 2018, 2019). Application of CRF significantly suppressed the early-sAHP/Ns slope to 31.8% of control value (from $0.22 \pm 0.05$ to $0.07 \pm 0.01$ mV/Ns; $n = 9$; $p = 0.002$; one-tailed Wilcoxon signed rank test; Fig. 1D) but did not significantly change the late-sAHP/Ns slope (from $0.05 \pm 0.01$ to $0.04 \pm 0.01$ mV/Ns; $n = 9$; $p = 0.082$; one-tailed Wilcoxon signed rank test; Fig. 1E). These results suggest that CRF enhances spike output by reducing preferentially the early-sAHP, which is partially dependent on the activation of $K_{Ca}$ channels (King et al., 2015; Tiwari et al., 2018, 2019). The late-sAHP, which is generated mostly by NKA activation (Gulledge et al., 2013; Tiwari et al., 2018), is unaffected by CRF.

We next examined the effect of CRF on the sAHPs evoked by stereotyped 3-s-long spike trains (Tiwari et al., 2018, 2019). Trains of 150 brief (2-ms-long) suprathreshold depolarizing pulses were delivered at 50 Hz to evoke sAHPs from a "holding" potential of $-70$ mV, evoking robust sAHPs (Fig. 2A). We measured the early- and late-sAHP amplitudes as described above, as well as the sAHP area (Fig. 2A; see Materials and Methods). Application of 250 nM CRF strongly suppressed the sAHPs (Fig. 2B). The early-sAHP amplitudes were significantly reduced to 51.1% of control size (from $-8.2 \pm 0.7$ to $-4.2 \pm 0.82$ mV; $n = 8$; $t = 5.44$; df = 7; $p = 0.001$; paired Student's $t$ test; Fig. 2C, left),

whereas the late-sAHP amplitudes were not significantly modified (from $-4.7 \pm 0.7$ to $-3.4 \pm 0.6$ mV; $n = 8$; $t = 2.11$; df = 7; $p = 0.07$; paired Student's $t$ test; Fig. 2C, middle). The sAHPs areas were also significantly suppressed by CRF to 58.6% of control size (from $-105.4 \pm 12.8$ to $-61.8 \pm 8.2$ mV•s; $t = 3.30$; df = 7; $p = 0.01$; $n = 8$; Fig. 2C, right). The magnitude of the CRF-induced reduction in early-sAHP amplitude was similar to that previously observed on acutely exchanging normal aCSF with Cd+Ni-aCSF (see Fig. 3 in Tiwari et al., 2018). Together, these results agree with the hypothesis that CRF preferentially suppresses the $K_{Ca}$-sAHP component while preserving the NKA-sAHP (Tiwari et al., 2019).

We tested the latter hypothesis in slices perfused for ~1 h with Cd+Ni-aCSF in which the sAHPs consist only of the NKA-sAHP component (Tiwari et al., 2018, 2019). The baseline size of the NKA-sAHPs was, on average, ~2 mV larger than that observed immediately after exchanging normal aCSF with Cd+Ni-aCSF (Tiwari et al., 2018), perhaps because of a slow facilitatory effect of the divalent cations on NKA activity. In this condition, application of 250 nM CRF still caused a mild (~4 mV) but significant depolarization of resting $V_m$ (from $-71.4 \pm 1.2$ to $-67.8 \pm 2.5$ mV; $n = 5$; $t = 3.9$; df = 4; $p = 0.0178$; paired Student's $t$ test). However, it had no significant effect on the AHPs (Fig. 2D; early-sAHP amplitudes: from $-6.3 \pm 1.2$ to $-5.8 \pm 0.38$ mV; $n = 5$; $t = 0.645$; df = 4; $p = 0.55$; paired Student's $t$ test; Fig. 2E, left; late-sAHP amplitudes: from $-4.1 \pm 0.47$ to $-3.2 \pm 0.54$ mV; $n = 5$; $t = 2.35$; df = 4; $p = 0.08$; Fig. 2E, middle; sAHP area: from $-83.2 \pm 13.7$ to $-76.5 \pm 10.8$ mV•s; $n = 5$;
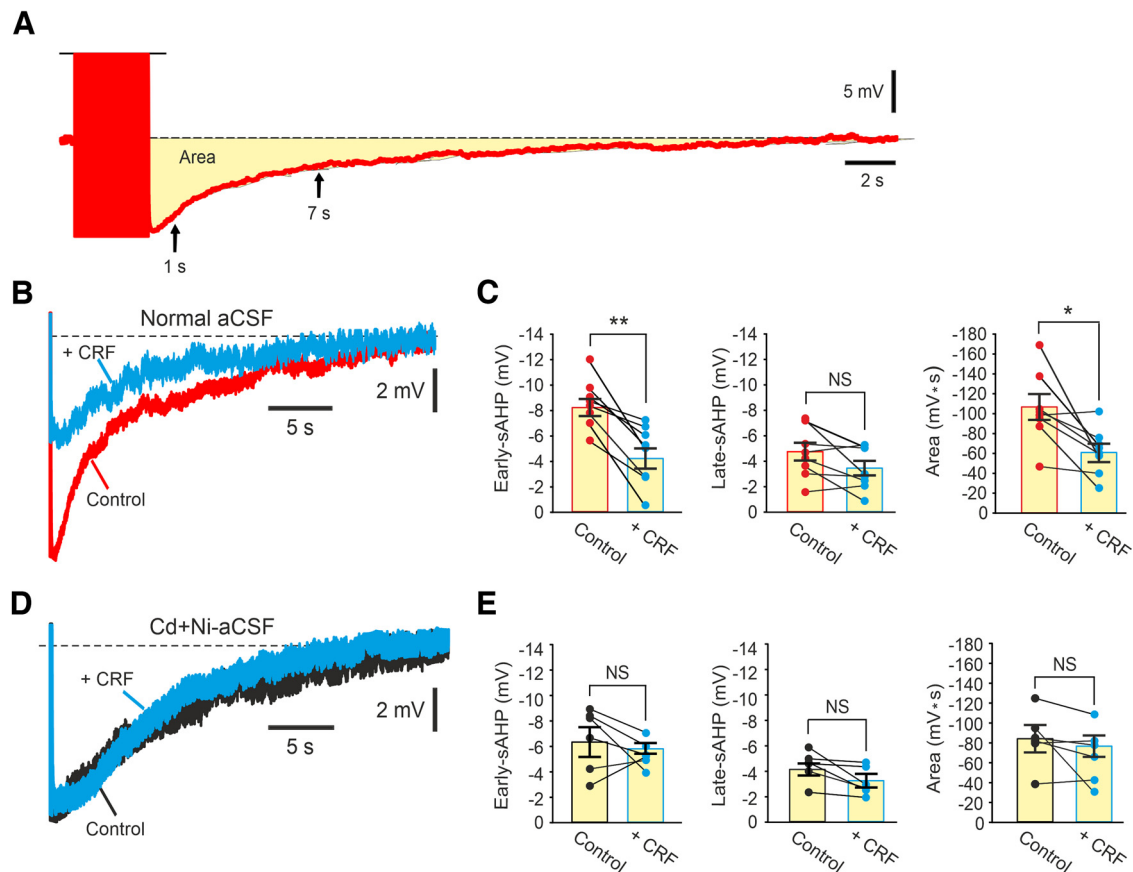
**Figure 2.** CRF suppresses the early, $Ca^{2+}$-dependent, sAHP phase of the dual-component sAHP in ordinary CA1 pyramidal cells. ***A***, A representative dual-component sAHP evoked by a stereotyped spike train stimulus (150 spikes at 50 Hz, for 3 s). The time points used to measure the early- and slow-sAHP amplitudes, as well as the "area under the curve" (integral) are depicted. ***B***, Representative overlaid traces of dual-component sAHPs evoked before (Control) and after CRF application (+ CRF). ***C***, Summary bar diagrams represent the early- and late-sAHP amplitudes, as well as the sAHP area, in the two conditions (*n* = 8). The early-sAHP amplitudes and the sAHP areas are significantly suppressed by CRF, but the late-sAHP amplitudes are unaffected. ***D***, Same as in ***B***, but the sAHPs were evoked in Cd + Ni-aCSF to block the $K_{Ca}$-sAHP component. ***E***, same as in ***C***, but bar diagrams apply to the experiments in Cd + Ni-aCSF (*n* = 5). In this condition, the sAHPs were unaffected by CRF. Data are mean ± SEM. \**p* < 0.05. \*\**p* < 0.01. NS, not significant.

$t = 1.53$; df = 4; $p = 0.2$; Fig. 2*E*, right). These results confirm that CRF does not interfere with NKA pump activity. They also suggest that the small CRF-induced depolarization is unrelated to the suppression of $K_{Ca}$ channels.

**CRF suppresses $K_{Ca}$-sAHP/$I_{sAHP}$ through a PKA-dependent action**
Isolation of $K_{Ca}$-sAHP from the dual-component sAHP can be achieved by inhibiting NKA transport activity with ouabain or with $K^+$-free aCSF (Tiwari et al., 2018). However, within ~20 min of NKA inhibition, the slices gradually deteriorate and cannot be subjected to further testing. In order to test the effect of CRF on stable $K_{Ca}$-sAHPs, we evoked "pure" $K_{Ca}$-sAHPs (in current-clamp mode; Fig. 3*A*, left) and $I_{sAHP}$s (in voltage-clamp mode; Fig. 3*A*, right) in slices perfused with TTX-aCSF (see Materials and Methods) (Tiwari et al., 2019). The peak amplitudes and durations of the $K_{Ca}$-sAHPs were −9.9 ± 1.0 mV and 4.3 ± 2.3 s, respectively (*n* = 12). In these neurons, the peak amplitudes of the $I_{sAHP}$s were 135.6 ± 17.6 pA.
Application of 250 nM CRF to the TTX-aCSF markedly and significantly suppressed the $K_{Ca}$-sAHPs to 16.7% of control size (from −10.6 ± 1.4 to −1.8 ± 0.6 mV; *n* = 5; *t* = 8.89; df = 4; *p* = 0.0009; paired Student's *t* test; Fig. 3*A*,*B*, left) without significantly affecting the rheobase currents and amplitudes of the $Ca^{2+}$ spikes (statistical data not shown; Fig. 3*A*, inset) Likewise, CRF markedly and significantly suppressed the $I_{sAHP}$s in these

neurons to 17.0% of control size (from 117.3 ± 16.3 to 19.9 ± 7.8 pA; *n* = 5; *t* = 8.36; df = 4; *p* = 0.001; paired Student's *t* test; Fig. 3*A*,*B*, right). These findings show that CRF suppresses the $K_{Ca}$-sAHPs by blocking their underlying $I_{sAHP}$.
Reduction of $I_{sAHP}$ by 250 nM CRF was previously demonstrated in CA1 pyramidal cells using patch-clamp recordings performed at room temperature (Haug and Storm, 2000). It was further shown that this effect depends on PKA activity. We have confirmed this finding also in our experimental condition by applying 250 nM CRF to slices pretreated with 10 μM H89, a PKA antagonist (Chijiwa et al., 1990). In this condition, CRF had no significant effect on $K_{Ca}$-sAHP amplitudes (from −8.9 ± 1.4 to −6.9 ± 0.8 mV; *n* = 6; *t* = 2.29; df = 5; *p* = 0.11; paired Student's *t* test; Fig. 3*C*,*D*, left) nor on $I_{sAHP}$ amplitudes (from 140.1 ± 22.0 to 103.6 ± 19.1 pA; *t* = 2.70; df = 5; *p* = 0.07; paired Student's *t* test; Fig. 3*C*,*D*, right). Likewise, no significant effects of CRF on the rheobase currents and amplitudes of the $Ca^{2+}$ spikes were noted also in this condition (statistical data not shown; Fig. 3*C*, inset).

**CRF suppresses $K_{Ca}$-sAHP/$I_{sAHP}$ via CRF₁Rs**
Hippocampal neurons express two isoforms of G-protein-coupled CRF receptors, namely, Type 1 ($CRF_1Rs$) and Type 2 receptors ($CRF_2Rs$) (Lovenberg et al., 1995; Perrin and Vale, 1999). Both receptors are expressed in the rat CA1 pyramidal layer (Chalmers et al., 1995). We tested which of the two CRF
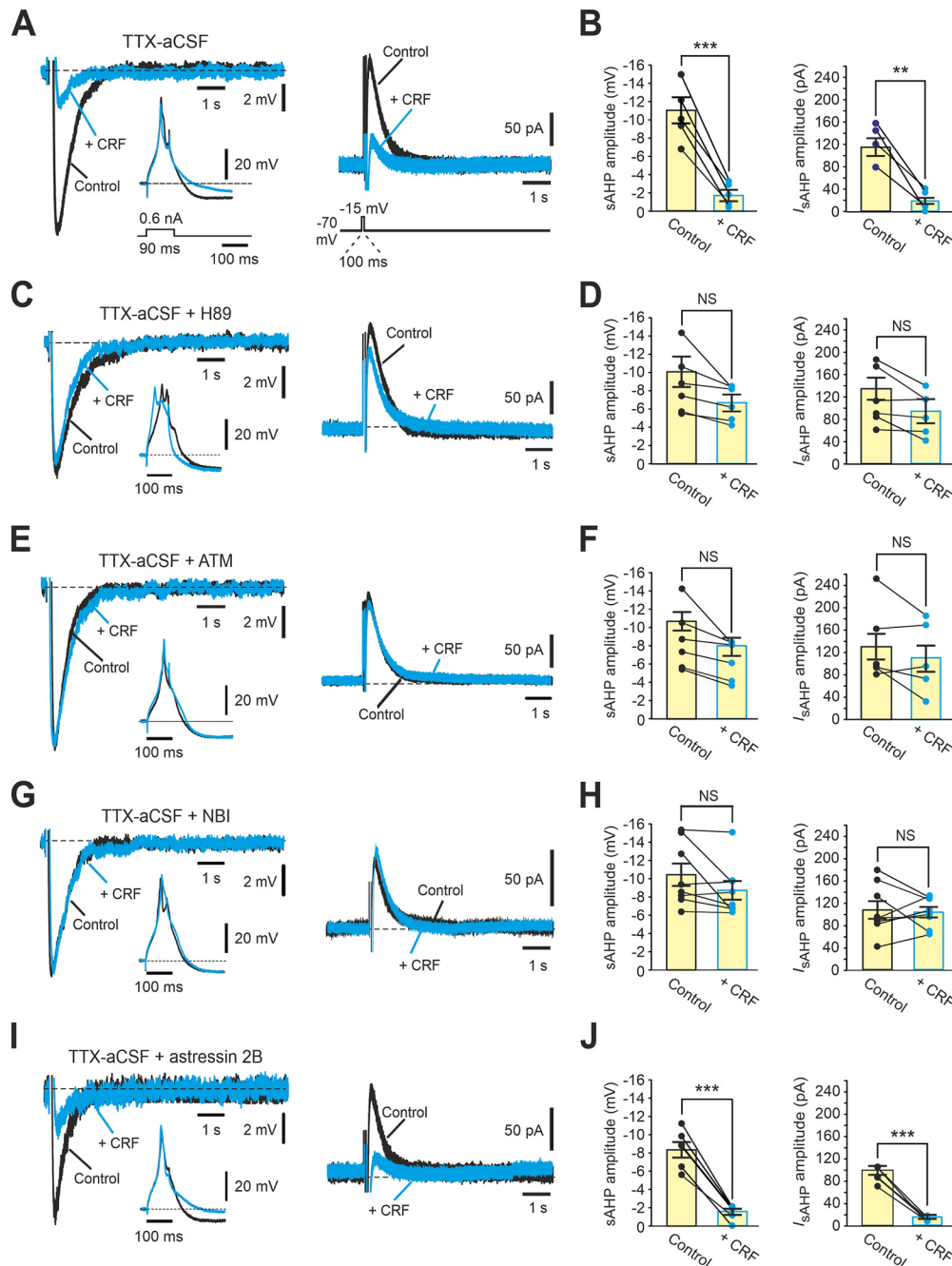
**Figure 3.** CRF suppresses $K_{Ca}$-sAHP/$I_{sAHP}$ via $CRF_1R$ and PKA in CA1 pyramidal cells. *A*, The effect of CRF on $K_{Ca}$-sAHP/$I_{sAHP}$ in a representative ordinary neuron. Left, Overlaid traces of $K_{Ca}$-sAHPs before (black) and after application of 250 nM CRF (blue). Inset, The respective $Ca^{2+}$ spikes generating the sAHPs (evoked, here and below, by 90-ms-long 0.6 nA depolarizing current pulses). Right, The overlaid traces represent the $I_{sAHP}$s in the same neuron (evoked, here and below, by 100-ms-long depolarizing pulses to −15 mV from a holding potential of −70 mV) before (black) and after CRF application (blue). The $K_{Ca}$-sAHP and the $I_{sAHP}$ are markedly suppressed by CRF, while the $Ca^{2+}$ spike is unaffected. *B*, Summary bar diagrams represent the suppressant effect of CRF on $K_{Ca}$-sAHP and $I_{sAHP}$ amplitudes in ordinary neurons (n = 5). *C*, Same as in *A*, but CRF was applied to slices treated with 10 μM H89, which prevented $K_{Ca}$-sAHP/$I_{sAHP}$ suppression. *D*, Summary bar diagrams represent the null effect of CRF on $K_{Ca}$-sAHP and $I_{sAHP}$ amplitudes in ordinary neurons in H89-treated slices (n = 6). *E*, Same as in *A*, but CRF was applied to slices treated with 1 μM ATM, which prevented $K_{Ca}$-sAHP/$I_{sAHP}$ suppression. *F*, Summary bar diagrams represent the null effect of CRF on $K_{Ca}$-sAHP (n = 6) and $I_{sAHP}$ amplitudes (n = 5) in ordinary neurons in ATM-treated slices. *G*, Same as in *A*, but CRF was applied to slices treated with 1 μM NBI27914, which prevented $K_{Ca}$-sAHP/$I_{sAHP}$ suppression. *H*, Summary bar diagrams represent the null effect of CRF on $K_{Ca}$-sAHP and $I_{sAHP}$ amplitudes in ordinary neurons in NBI27914-treated slices (n = 8). *I*, Same as in *A*, but CRF was applied to slices treated with 250 nM astressin 2B, which did not prevent $K_{Ca}$-sAHP/$I_{sAHP}$ suppression. *J*, Summary bar diagrams represent the suppressant effect of CRF on $K_{Ca}$-sAHP and $I_{sAHP}$ amplitudes in ordinary neurons in astressin 2B-treated slices (n = 6). Data are mean ± SEM. **p < 0.01. ***p < 0.001. NS, not significant.

receptors is involved in CRF-induced $K_{Ca}$-sAHP/$I_{sAHP}$ suppression using selective CRF receptor antagonists.

In slices treated 1 μM ATM, a $CRF_1R$ antagonist (Webster et al., 1996; Habib et al., 2000), CRF application did not significantly modify $K_{Ca}$-sAHP amplitudes (from −9.6 ± 0.5 to −8.0 ± 0.8 mV; n = 6; t = 1.76; df = 5; p = 0.14; paired Student's t test; Fig. 3E,F, left)

nor $I_{sAHP}$ amplitudes (from 128.9 ± 24.9 to 109.7 ± 24.4 pA; n = 5; t = 1.52; df = 4; p = 0.20; paired Student's t test; Fig. 3E,F, right). Similarly, in slices treated with 1 μM NBI27194 (NBI), also a selective $CRF_1R$ antagonist (Chen et al., 1996), CRF application did not significantly modify $K_{Ca}$-sAHP (from −10.4 ± 1.2 to −8.7 ± 1.0 mV; n = 8; t = 1.891; df = 7; p = 0.10; paired Student's
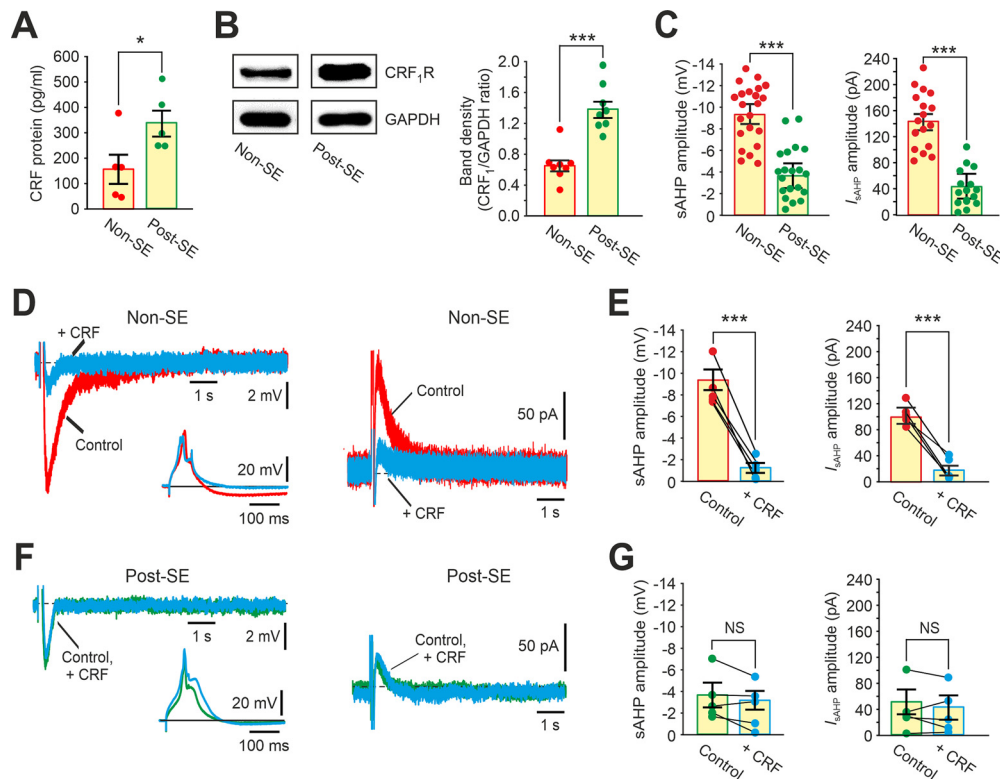
**Figure 4.** Upregulation of CRF/CRF$_1$R protein expression in epileptogenesis accounts for K$_{Ca}$-sAHP/I$_{sAHP}$ suppression in post-SE neurons and occludes the action of exogenous CRF. ***A***, Summary bar diagram represents CRF protein expression measured by ELISA in hippocampal tissue of non-SE and post-SE rats (5 rats in each group). CRF expression is significantly upregulated in the latter group. ***B***, Left, Representative Western blots of CRF$_1$R protein (47 kDa) and GAPDH protein (serving as control; 37 kDa) obtained from hippocampal tissue of non-SE and post-SE rats. Note higher band density of CRF$_1$R protein in post-SE hippocampal tissue. Right, Summary bar diagram represents the CRF$_1$R/GAPDH band density ratios in non-SE (8 rats) and post-SE hippocampal tissues (8 rats). The ratio is significantly higher in the post-SE tissue, indicating significant CRF$_1$R protein upregulation. ***C***, Summary bar diagrams comparing K$_{Ca}$-sAHP amplitudes (left) and I$_{sAHP}$ amplitudes (right) in non-SE versus post-SE neurons. ***D***, The effect of CRF on a representative non-SE neuron. Left, Overlaid traces of K$_{Ca}$-sAHPs before (red) and after application of 250 nM CRF (blue). Inset, The respective Ca$^{2+}$ spikes generating the sAHPs. Right, The overlaid traces represent the I$_{sAHP}$s in the same neuron before (red) and after CRF application (blue). The K$_{Ca}$-sAHP and the I$_{sAHP}$ are markedly suppressed by CRF, while the Ca$^{2+}$ spike is unaffected. ***E***, Summary bar diagrams represent the suppressant effect of CRF on K$_{Ca}$-sAHP ($n = 5$) and I$_{sAHP}$ amplitudes ($n = 5$) in non-SE neurons ($n = 5$). ***F***, Same as in ***D***, but CRF was applied to post-SE neurons. The control K$_{Ca}$-sAHP/I$_{sAHP}$ amplitudes (green) are smaller than in non-SE neurons because of epileptogenesis, occluding the effect of exogenous CRF (blue). ***G***, Summary bar diagrams represent the lack of additional effect of CRF on K$_{Ca}$-sAHP and I$_{sAHP}$ amplitudes in post-SE neurons ($n = 5$). Data are mean ± SEM. ***$p < 0.001$. NS, not significant.

$t$ test) nor I$_{sAHP}$ amplitudes (from 107.9 ± 15.9 to 102.0 ± 9.4 pA; $n = 8$; $t = 0.443$; df = 7; $p = 0.671$; paired Student's $t$ test; Fig. 3*G,H*). Neither ATM (Fig. 3*E*, inset) nor NBI (Fig. 3*G*, inset) significantly affected the rheobase currents and amplitudes of the Ca$^{2+}$ spikes (statistical data not shown).

In contrast, in slices treated with 250 nM astressin 2B, a CRF$_2$ antagonist (Rivier et al., 2002), CRF application strongly and significantly suppressed both K$_{Ca}$-sAHP to 18.6% of control size (from −8.4 ± 0.9 to −1.6 ± 0.3 mV; $n = 6$; $t = 10.94$; df = 5; $p = 0.0001$; paired Student's $t$ test) and I$_{sAHP}$ to 14.2% of control size (from 88.8 ± 5.3 to 12.6 ± 1.5 pA; $n = 6$; $t = 14.29$; df = 5; $p = 0.0001$; paired Student's $t$ test; Fig. 3*I,J*). No effects of CRF on Ca$^{2+}$ spike rheobase currents and amplitudes were noted also in this condition (statistical data not shown; Fig. 3*I*, inset).

These results establish CRF$_1$Rs as mediators of PKA-dependent K$_{Ca}$-sAHP/I$_{sAHP}$ suppression by CRF.

### CRF and CRF$_1$R expression in hippocampi of non-SE versus post-SE rats
Given that CRF/CRF$_1$R/PKA signaling downregulates K$_{Ca}$-sAHPs/I$_{sAHP}$s in CA1 pyramidal cells, we tested whether this pathway is upregulated in our model of acquired TLE. To that end, we first compared CRF and CRF$_1$R protein expression in chronic non-SE versus post-SE hippocampus. The expression of CRF protein was

measured using ELISA (see Materials and Methods). We found that CRF protein levels were considerably (214.2%) higher in post-SE hippocampal tissue compared with non-SE tissue (343.5 ± 51.7 vs 160.4 ± 58.9 pg/ml, respectively; 5 rats in each group; $t = 2.34$; df = 8; $p = 0.04$; unpaired Student's $t$ test; Fig. 4*A*).

Next, we measured CRF$_1$R protein expression using Western blotting (see Materials and Methods). Similarly, we found a marked (212.4%) increase in expression of the latter protein (normalized to GAPDH expression) in post-SE versus non-SE tissues (CRF$_1$R/GAPDH ratios: 1.4 ± 0.1 vs 0.7 ± 0.1, respectively; $n = 8$ rats in each group; $t = 5.6$; df = 14; $p = 0.0001$; unpaired Student's $t$ test Fig. 4*B*).

These findings, showing enhanced CRF/CRF$_1$R expression in post-SE hippocampal tissue, suggested that CRF/CRF$_1$R/PKA signaling may be upregulated in post-SE neurons, thus leading to the observed K$_{Ca}$-sAHPs/I$_{sAHP}$s downregulation and intrinsic hyperexcitability in these neurons. Therefore, we further explored the role of CRF in these TLE-related alterations.

### Effects of CRF on K$_{Ca}$-sAHP/I$_{sAHP}$ in non-SE and post-SE neurons
We next tested how CRF affects the K$_{Ca}$-sAHPs and I$_{sAHP}$s in non-SE and post-SE CA1 pyramidal cells. As previously described (Tiwari et al., 2019), the CA1 pyramidal cells in the

non-SE group displayed $K_{Ca}$-sAHPs and $I_{sAHP}$s similar in size to those recorded in neurons of naive rats. Also, $K_{Ca}$-sAHP amplitudes in post-SE neurons were remarkably (40.0%) smaller than those recorded in non-SE neurons ($n = 25$ and $n = 22$, respectively; $-3.8 \pm 0.5$ vs $-9.4 \pm 0.6$ mV, respectively; $t = 7.058$; df = 45; $p = 0.0001$; unpaired Student's $t$ test; Fig. 4C, left). Likewise, $I_{sAHP}$ amplitudes were also much (28.3%) smaller than those recorded in non-SE neurons ($n = 20$ and $n = 20$, respectively; $40.2 \pm 5.9$ vs $142.3 \pm 9.5$ pA, respectively; $t = 9.121$; df = 38; $p = 0.0001$; unpaired Student's $t$ test; Fig. 4C, right). The $Ca^{2+}$ spike rheobase currents and amplitudes were similar in the two groups (statistical data not shown) (Tiwari et al., 2019).

As in naive neurons (Fig. 3A,B), application of 250 nM CRF to non-SE neurons similarly caused a significant suppression of both $K_{Ca}$-sAHPs (to 13.1% of control size; from $-8.7 \pm 0.9$ to $-1.1 \pm 0.4$ mV; $n = 5$, $t = 12.5$; df = 4; $p = 0.0002$; paired Student's $t$ test) and $I_{sAHP}$s (to 20.3% of control size; from $103.2 \pm 7.2$ to $21.0 \pm 7.3$ pA; $n = 5$; $t = 9.8$; df = 4; $p = 0.0006$; paired Student's $t$ test; Fig. 4D,E). In contrast, applying CRF to post-SE neurons had no significant effect on the amplitudes of the residual $K_{Ca}$-sAHPs (from $-3.3 \pm 1.0$ to $-2.6 \pm 0.9$ mV; $n = 5$; $t = 1.746$; df = 4; $p = 0.156$; paired Student's $t$ test) and $I_{sAHP}$s (from $39.4 \pm 16.2$ to $36.4 \pm 15.3$ pA; $n = 5$; $t = 0.492$; df = 5; $p = 0.65$; paired Student's $t$ test; Fig. 4F,G).

These findings suggest that the suppressant effect of exogenous CRF on $K_{Ca}$-sAHPs/$I_{sAHP}$s is occluded in post-SE neurons, possibly because of enhanced CRF/CRF$_1$R/PKA signaling in these neurons.

## Recovery of $K_{Ca}$-sAHP/$I_{sAHP}$ in post-SE neurons by CRF$_1$R antagonists

Because PKA inhibitors were shown to restore $K_{Ca}$-sAHPs/$I_{sAHP}$s amplitudes and to normalize the excitability of post-SE neurons (Tiwari et al., 2019), we next tested whether CRF$_1$R antagonists would act in a similar fashion. The amplitudes of the $K_{Ca}$-sAHPs in 1 μM ATM-treated post-SE neurons were slightly but significantly smaller than in ATM-treated non-SE neurons ($-7.0 \pm 0.3$ mV, $n = 13$ vs $-8.5 \pm 0.6$ mV; $n = 12$, respectively; $t = 2.521$; df = 23; $p = 0.02$; unpaired Student's $t$ test; Fig. 5A,B, top), as were the amplitudes of the $I_{sAHP}$s ($85.2 \pm 4.8$ pA, $n = 11$ vs $118.5 \pm 7.8$ pA, $n = 12$, respectively; $t = 3.568$; df = 21; $p = 0.002$; unpaired Student's $t$ test $p = 0.002$; Fig. 5A,B, bottom). Slightly different results were obtained with NBI. The amplitudes of the $K_{Ca}$-sAHPs in 1 μM NBI-treated post-SE neurons were similar to those in NBI-treated non-SE neurons ($-7.8 \pm 0.6$ mV, $n = 14$ vs $-7.7 \pm 0.7$ mV, $n = 9$, respectively; $t = 0.12$; df = 21; $p = 0.91$; unpaired Student's $t$ test; Fig. 4C,D, top), as were the amplitudes of the $I_{sAHP}$s ($81 \pm 5.2$ pA, $n = 13$ vs $77.0 \pm 9.4$ pA, $n = 9$, respectively; $t = 0.521$; df = 20; $p = 0.61$; unpaired Student's $t$ test; Fig. 4C,D, bottom). The $Ca^{2+}$ spike rheobase currents and amplitudes in ATM-treated non-SE and post-SE neurons were the same, as was the case in NBI-treated neurons (statistical data not shown).

Further comparisons of $K_{Ca}$-sAHPs and $I_{sAHP}$s amplitudes within the non-SE groups indicated that ATM treatment has no effect on these amplitudes, whereas NBI treatment reduces them, respectively, to 81.4% and 54.2% of the untreated group values (although only the reduction in $I_{sAHP}$s amplitudes attained statistical significance; $K_{Ca}$-sAHPs: $F = 1.597$; $R^2 = 0.06915$; $p = 0.2142$; $I_{sAHP}$s: $F = 10.78$; $R^2 = 0.3619$; $p = 0.0002$; one-way ANOVA; Fig. 5E). An NBI-induced $I_{sAHP}$s reduction was also noted in NBI-treated naive neurons; see Fig. 3G. Thus, NBI may exert also a partial agonistic action at CRF$_1$Rs in addition to full antagonism of CRF action.

Similar comparisons within the post-SE groups indicated that $K_{Ca}$-sAHPs and $I_{sAHP}$s amplitudes were, respectively, 184.2% and 211.4% larger in ATM-treated post-SE neurons than in the untreated group. Likewise, these amplitudes were, respectively, 205.3% and 202.3% larger in the NBI-treated post-SE neurons than in the untreated group ($K_{Ca}$-sAHPs: $F = 19.88$; $R^2 = 0.4636$; $p = 0.0001$; $I_{sAHP}$s: $F = 15.07$; $R^2 = 0.4237$; $p = 0.0001$; one-way ANOVA; Fig. 5F).

Together, these results indicate that CRF$_1$R antagonists are able to acutely restore most (ATM), if not all (NBI), of the $K_{Ca}$-sAHPs/$I_{sAHP}$s in post-SE CA1 pyramidal cells.

## Effects of TRAM-34 on restored $K_{Ca}$-sAHP/$I_{sAHP}$ in post-SE neurons

Recent studies have shown that the $K_{Ca}$ channels generating the $K_{Ca}$-sAHPs/$I_{sAHP}$s in hippocampal and cortical pyramidal cells are the intermediate conductance $K_{Ca}$3.1 channels (King et al., 2015; Turner et al., 2016; Sahu et al., 2019; Roshchin et al., 2020; for review, see Sahu and Turner, 2021). In support of this hypothesis, it was shown that $K_{Ca}$3.1 channels are expressed by CA1 pyramidal cells (Turner et al., 2015) and that the $I_{sAHP}$ in these neurons is suppressed by TRAM-34 (King et al., 2015; Turner et al., 2016; Tiwari et al., 2018, 2019), a selective blocker of $K_{Ca}$3.1 channels (Wulff et al., 2000). We have also shown previously that the $K_{Ca}$-sAHPs/$I_{sAHP}$s restored in post-SE neurons by PKA inhibitors are suppressed by TRAM-34, indicating that they are generated by native $K_{Ca}$3.1 channels (Tiwari et al., 2019). We tested the latter notion further by examining the TRAM-34 sensitivity of the $K_{Ca}$-sAHPs/$I_{sAHP}$s restored by the CRF$_1$R antagonists.

In 1 μM ATM-treated non-SE neurons, application of 5 μM TRAM-34 strongly and significantly reduced $K_{Ca}$-sAHP amplitudes (to 17.2% of control size; $n = 6$; from $-9.3 \pm 0.6$ to $-1.6 \pm 0.3$ mV; $t = 11.524$; df = 5; $p = 0.0001$; paired Student's $t$ test) and $I_{sAHP}$ amplitudes (to 8.5% of control size; $n = 6$; from $121.7 \pm 8.0$ to $10.4 \pm 2.2$ pA; $t = 14.55$; df = 5; $p = 0.0001$; paired Student's $t$ test; Fig. 6A,B). In ATM-treated post-SE neurons, TRAM-34 also strongly and significantly suppressed both $K_{Ca}$-sAHP (to 18.3% of control size; $n = 6$; from $-6.5 \pm 0.5$ to $-1.2 \pm 0.4$ mV; $t = 40.03$; df = 5; $p = 0.0001$; paired Student's $t$ test) and $I_{sAHP}$ amplitudes (to 9.4% of control size; $n = 6$; from $100.3 \pm 23.7$ to $9.5 \pm 1.0$ pA; $t = 8.84$; df = 5; $p = 0.009$; paired Student's $t$ test; Fig. 6C,D).

Similar results were obtained in neurons in slices treated with 1 μM NBI. In non-SE neurons, TRAM-34 application strongly and significantly reduced $K_{Ca}$-sAHP (to 16.6% of control size; from $-7.7 \pm 1.0$ to $-1.3 \pm 0.6$ mV; $t = 10.13$; df = 5; $p = 0.0002$; paired Student's $t$ test) and $I_{sAHP}$ amplitudes (to 22.6% of control size; from $77.8 \pm 14.1$ to $17.6 \pm 4.0$ pA; $t = 5.03$; df = 5; $p = 0.004$; paired Student's $t$ test; Fig. 6E,F). Likewise, in post-SE neurons, TRAM-34 strongly and significantly suppressed both $K_{Ca}$-sAHP amplitudes (to 23.1 of control size; $n = 7$; from $-7.3 \pm 1.0$ to $-1.7 \pm 0.7$ mV; $t = 7.06$; df = 6; $p = 0.0004$; paired Student's $t$ test) and $I_{sAHP}$ amplitudes (to 19.4 of control size; $n = 7$; from $83.2.0 \pm 8.2$ to $16.1 \pm 5.6$ pA; $t = 7.341$; df = 6; $p = 0.0003$; paired Student's $t$ test; Fig. 6G,H). Similar to previous findings (Tiwari et al., 2019), no significant effects of TRAM-34 on $Ca^{2+}$ spike rheobase currents and spike amplitudes were observed in the four groups of neurons (statistical data not shown).

The sensitivity of the restored $K_{Ca}$-sAHPs/$I_{sAHP}$s to TRAM-34 indicates that $K_{Ca}$-sAHPs/$I_{sAHP}$s downregulation in post-SE
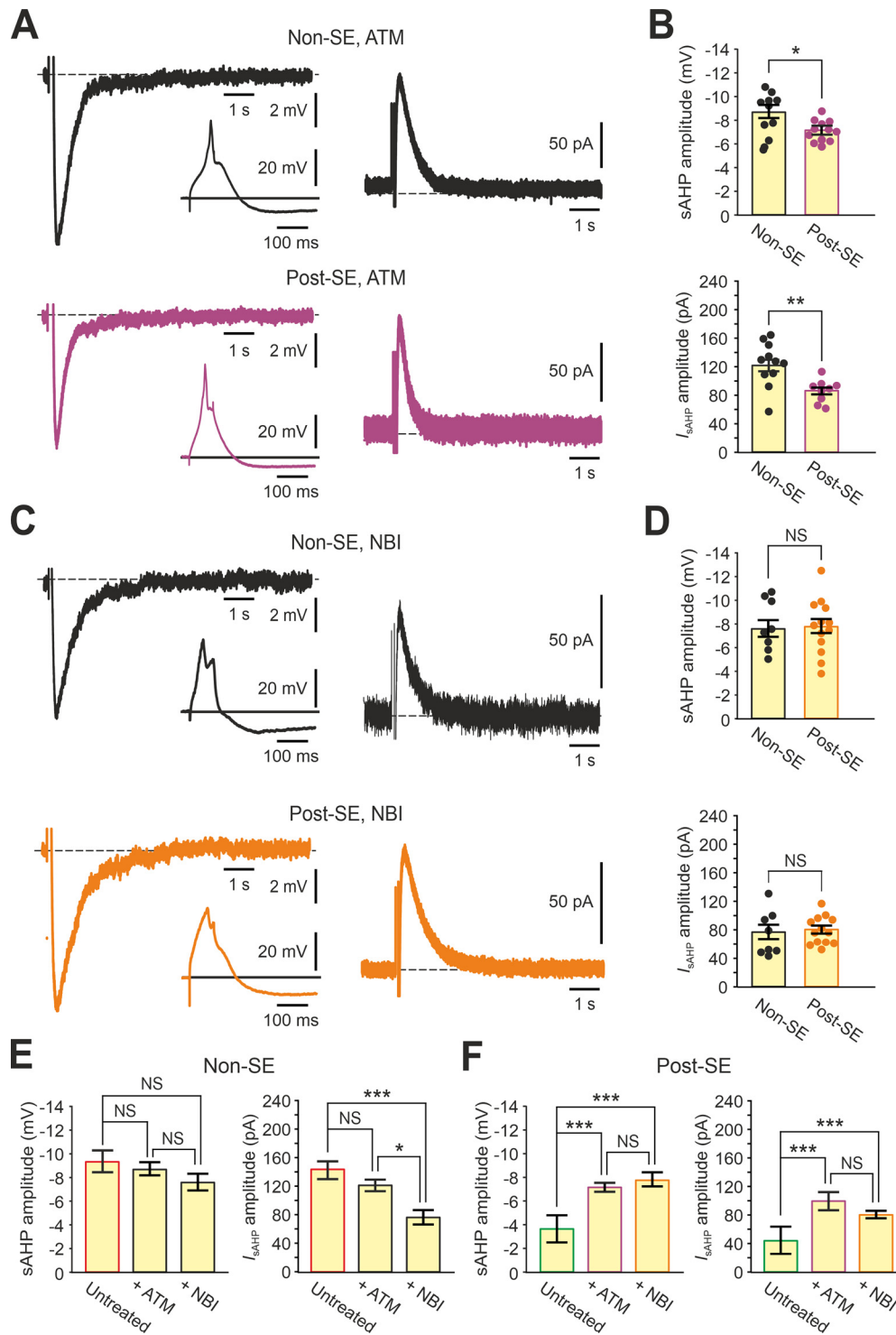
**Figure 5.** CRF$_1$R antagonists restore K$_{Ca}$-sAHP/I$_{sAHP}$ in post-SE neurons. ***A***, The K$_{Ca}$-sAHP (left) and the I$_{sAHP}$ (right) recorded in representative non-SE (top traces, black) and post-SE neurons (bottom traces, violet) in slices treated with 1 $\mu$M ATM. Insets, The Ca$^{2+}$ spikes evoking the K$_{Ca}$-sAHP. ***B***, Summary bar diagrams of K$_{Ca}$-sAHP (top) and I$_{sAHP}$ amplitudes (bottom) recorded in non-SE ($n = 12$ and $n = 12$, respectively) and post-SE neurons ($n = 13$ and $n = 11$, respectively) in ATM-treated slices. In both diagrams, the amplitudes in post-SE neurons are significantly smaller than in non-SE nears, implying only a partial K$_{Ca}$-sAHP/I$_{sAHP}$ restoration by ATM. ***C***, Same as in ***A***, but for neurons recorded in slices treated with 1 $\mu$M NBI. ***D***, Summary bar diagrams K$_{Ca}$-sAHP (top) and I$_{sAHP}$ amplitudes (bottom) recorded in non-SE ($n = 9$ and $n = 9$, respectively) and post-SE neurons ($n = 14$ and $n = 13$, respectively) in NBI-treated slices. In both diagrams, the K$_{Ca}$-sAHP/I$_{sAHP}$ amplitudes recorded in non-SE and post-SE neurons are the same, implying a complete K$_{Ca}$-sAHP/I$_{sAHP}$ restoration by NBI. ***E***, Summary bar diagrams of K$_{Ca}$-sAHP (left) and I$_{sAHP}$ amplitudes (right) recorded in non-SE neurons in untreated ($n = 25$ and $n = 20$, respectively), in ATM-treated ($n = 12$ in both) and in NBI-treated slices ($n = 9$ in both). NBI, but not ATM, significantly reduces I$_{sAHP}$ amplitudes in non-SE neurons. ***F***, Summary bar diagrams of K$_{Ca}$-sAHP (left) and I$_{sAHP}$ amplitudes (right) recorded in post-SE neurons in untreated ($n = 22$ and $n = 20$, respectively), in ATM-treated ($n = 13$ and $n = 11$, respectively) and in NBI-treated slices ($n = 14$ and $n = 13$, respectively). Application of either ATM or NBI significantly restores K$_{Ca}$-sAHP/I$_{sAHP}$ in post-SE neurons. Data are mean $\pm$ SEM. *$p < 0.05$. **$p < 0.01$. ***$p < 0.001$. NS, not significant.
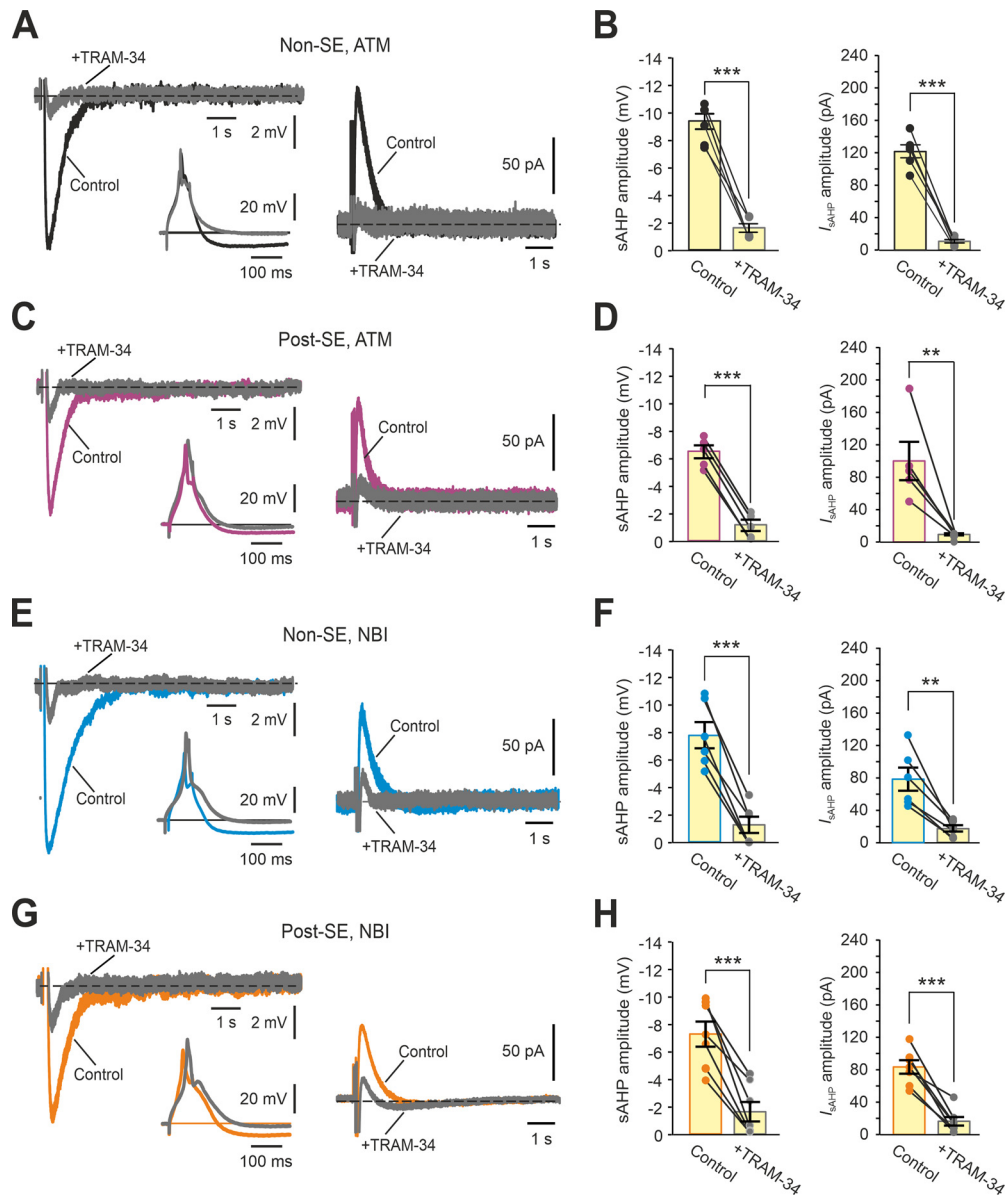
**Figure 6.** TRAM-34 similarly suppresses native $K_{Ca}$-sAHP/$I_{sAHP}$ in non-SE neurons and restored $K_{Ca}$-sAHP/$I_{sAHP}$ in post-SE neurons. **A**, The effect of TRAM-34 on native $K_{Ca}$-sAHP/$I_{sAHP}$ in a representative non-SE neuron in slices treated with 1 $\mu$M ATM. Left, Overlaid traces of $K_{Ca}$-sAHPs before (black) and after application of 5 $\mu$M TRAM-34 (gray). The respective $Ca^{2+}$ spikes generating the sAHPs are shown in the inset. Right, The overlaid traces represent the $I_{sAHP}$s in the same neuron before (black) and after TRAM-34 application (gray). The $K_{Ca}$-sAHP and the $I_{sAHP}$ are markedly suppressed by TRAM-34, while the $Ca^{2+}$ spike is unaffected. **B**, Summary bar diagrams represent the suppressant effect of TRAM-34 on native $K_{Ca}$-sAHP and $I_{sAHP}$ amplitudes in ATM-treated non-SE neurons ($n = 6$). **C**, Same as in **A**, but TRAM-34 was applied to ATM-treated post-SE slices. The restored $K_{Ca}$-sAHPs and $I_{sAHP}$s (violet traces) were suppressed by TRAM-34 (gray traces). **D**, Summary bar diagrams represent the suppressant effect of CRF on restored $K_{Ca}$-sAHP and $I_{sAHP}$ amplitudes in ATM-treated post-SE slices ($n = 6$). **E**, Same as in **A**, but TRAM-34 was applied to non-SE slices treated with 1 $\mu$M NBI. The native $K_{Ca}$-sAHPs and $I_{sAHP}$s (blue traces) were suppressed by TRAM-34 (gray traces). **F**, Summary bar diagrams represent the suppressant effect of CRF on native $K_{Ca}$-sAHP and $I_{sAHP}$ amplitudes in NBI-treated post-SE slices ($n = 6$). **G**, Same as in **A**, but TRAM-34 was applied to NBI-treated post-SE slices. The restored $K_{Ca}$-sAHPs and $I_{sAHP}$s (orange traces) were suppressed by TRAM-34 (gray traces). **H**, Summary bar diagrams represent the suppressant effect of CRF on restored $K_{Ca}$-sAHP and $I_{sAHP}$ amplitudes in NBI-treated post-SE slices ($n = 7$). **$p < 0.01$. ***$p < 0.001$.

neurons is because of CRF/CRF$_1$R/PKA-mediated inhibition of $K_{Ca}$3.1 channels.

### CRF$_1$R antagonists normalize the dual-component sAHP in post-SE neurons

We have previously shown that the early-sAHP amplitudes of the dual-component sAHPS are smaller in post-SE than in non-SE CA1 pyramidal cells (Tiwari et al., 2019). Given that these amplitudes are selectively reduced by CRF in ordinary neurons (Fig. 2B,C) in a $Ca^{2+}$-dependent manner (Fig. 2D,E), we tested whether their reduction in post-SE

neurons is because of CRF-mediated suppression of the $K_{Ca}$-sAHPs/$I_{sAHP}$s. To that end, we evoked dual-component sAHPs in slices perfused with standard aCSF using the 150 spikes-train protocol (Fig. 2A). The early-sAHP amplitudes in untreated non-SE neurons were significantly bigger compared with those in post-SE neurons ($-9.2 \pm 0.6$ mV, $n = 27$ vs $-5.9 \pm 0.4$ mV, $n = 37$, respectively; $t = 4.51$; df = 62; $p = 0.0001$; unpaired Student's $t$ test; Fig. 7A,B, left). No differences in late-sAHP amplitudes ($-4.0 \pm 0.3$ vs $-4.1 \pm 0.2$ mV, respectively; $t = 0.22$; df = 62; $p = 0.83$; unpaired Student's $t$ test; Fig. 7A,B, middle) and in sAHP areas ($-104.5 \pm 7.3$ vs
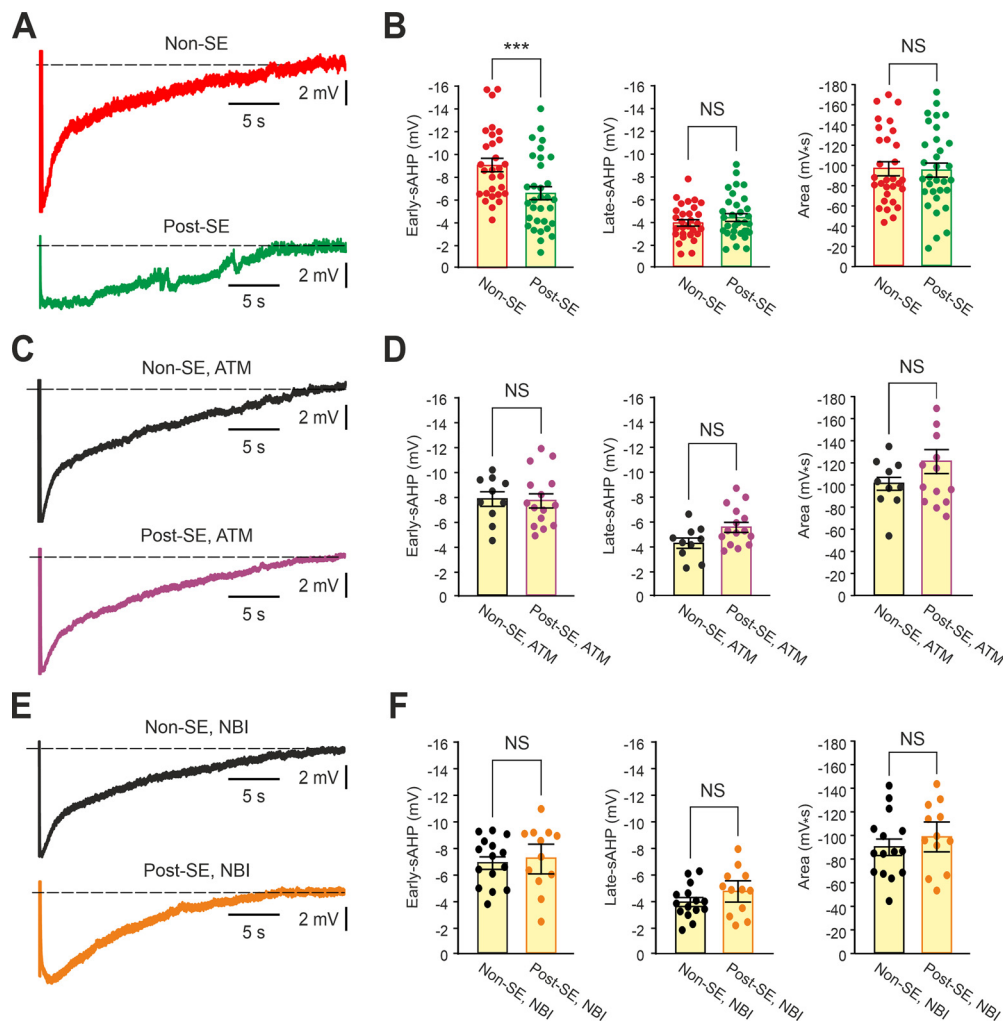
**Figure 7.** CRF₁R antagonists restore the early-sAHP component of dual-component sAHPs evoked by stereotyped spike-trains in post-SE neurons. **A**, The dual-component sAHPs (evoked by a train of 150 spikes, 50 Hz) recorded in representative non-SE (top trace, red) and post-SE neurons (bottom trace, green). **B**, Summary bar diagrams comparing (from left to right) the amplitudes of the early-sAHP, the late-sAHP, and the sAHP area, in untreated non-SE (n = 27) and post-SE neurons (n = 37). The early-sAHPs in post-SE neurons are smaller in amplitude than their non-SE counterparts. **C**, Same as in **A**, but for neurons recorded in slices treated with 1 μM ATM. **D**, Same as in **B**, but for non-SE (n = 10) and post-SE neurons (n = 15) in ATM-treated slices. The early-sAHP is normalized by ATM. **E**, Same as in **A**, but for neurons recorded in slices treated with 1 μM NBI. **F**, Same as in **B**, but for non-SE (n = 15) and post-SE neurons (n = 12) in NBI-treated slices. The early-sAHP is normalized by NBI. ***p < 0.001. NS, not significant.

−92.0 ± 4.2 mV•s; t = 1.49; df = 62; p = 0.14; Fig. 7A,B, right) were observed between these non-SE and post-SE neurons.

In contrast, the early-sAHP amplitudes in 1 μM ATM-treated non-SE and post-SE neurons were similar (−7.8 ± 0.6 mV, n = 10 vs −7.8 ± 0.6 mV, n = 15, respectively; t = 0.054; df = 23; p = 0.96; unpaired Student's t test; Fig. 7C,D, left), as were the late-sAHP amplitudes (−4.3 ± 0.4 vs −5.3 ± 0.3 mV, respectively; t = 1.91; df = 23; p = 0.07; unpaired Student's t test; Fig. 7C,D, middle) and sAHP areas (−100.8 ± 7 and −121.7 ± 10.9 mV•s, respectively; t = 1.43; df = 23; p = 0.17; unpaired Student's t test; Fig. 7C,D, right). Likewise, the early-sAHP amplitudes in 1 μM NBI-treated non-SE and post-SE neurons were similar (−6.9 ± 0.5, n = 15 vs −7.2 ± 1.1 mV, n = 12, respectively; t = 0.40; df = 25; p = 0.69; unpaired Student's t test; Fig. 7E,F, left), as were the late-sAHP amplitudes (−3.9 ± 0.3 vs −4.87 ± 0.8 mV, respectively; t = 1.38; df = 25; p = 0.18; unpaired Student's t test; Fig. 7E,F, middle) and sAHP areas (−89.8 ± 7.0 and −98.6 ± 12.6 mV•s, respectively; t = 0.82; df = 25; p = 0.42; unpaired Student's t test; Fig. 7E,F, right). Thus, CRF₁R antagonism normalizes the dual-component sAHPs in post-SE neurons.

**CRF₁R antagonism normalizes the intrinsic excitability of post-SE neurons**
Next, we tested whether sAHP normalization by CRF₁R antagonists also counteracts the hyperexcitability of post-SE CA1 pyramidal cells, expressed as increased spike response gain (Tamir et al., 2017; Tiwari et al., 2019). To that end, recordings were made in slices perfused with standard aCSF, and spike activity was elicited by 1-s-long depolarizing current pulses, as described above (Fig. 1A). The firing responses and dual-component sAHPs evoked by 0.3 nA pulses in representative control non-SE and post-SE neurons are shown in Figure 8A, B. The spike output gain values in post-SE neurons were significantly higher than in non-SE neurons (71.5 ± 7.9 Ns/I, n = 11 vs 33.5 ± 4.5 Ns/I, n = 15, respectively; p = 0.00002; Mann–Whitney test; Fig. 8C). Additionally, consistent with the above findings (Fig. 7A,B), the early-sAHPs following the spike responses were significantly smaller in post-SE compared with non-SE slices (0.1 ± 0.02 vs 0.33 ± 0.05 mV/Ns, respectively; p = 0.0002; Mann–Whitney test; Fig. 8D), whereas the late-sAHPs were the same (0.05 ± 0.01 vs 0.07 ± 0.01 mV/Ns, respectively; p = 0.47; Mann–Whitney test; Fig. 8E).
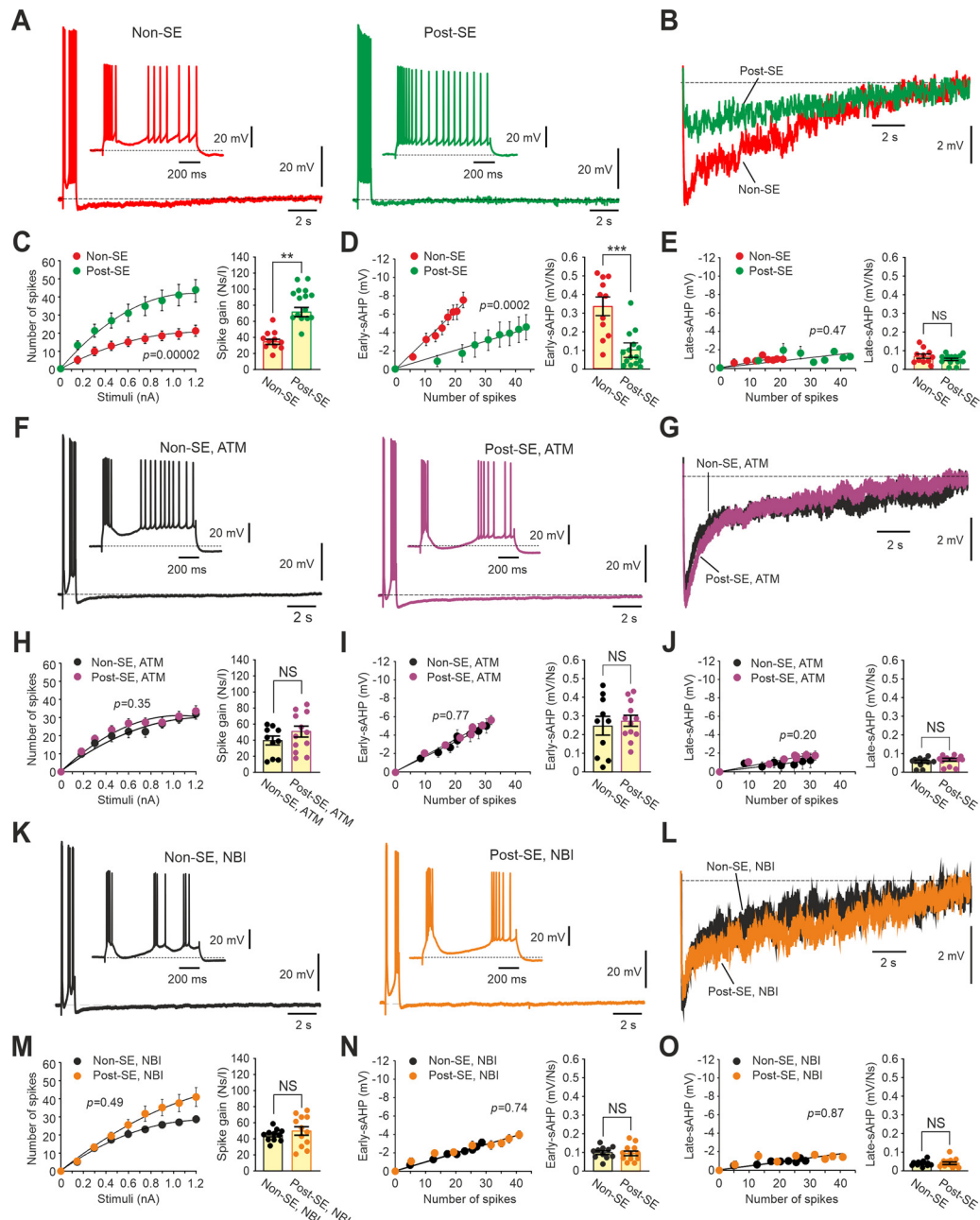
**Figure 8.** CRF$_1$R antagonists normalize the excitability of post-SE neurons while restoring early-sAHP. ***A***, Representative traces depict at two time scales the firing of a non-SE (left) and a post-SE CA1 pyramidal cell (right) stimulated by a 1-s-long depolarizing current pulse (0.3 nA). ***B***, Overlaid enlarged traces of the sAHPs generated by the non-SE (red) and post-SE (green) neurons shown in ***A***. ***C***, Summary plots represent the number of evoked spikes (Ns) as a function of stimulation intensity (I) in non-SE ($n = 11$) and post-SE neurons ($n = 15$). Bar diagram represents the spike response gains (Ns/I) in the two groups of neurons. The gain is significantly larger in the post-SE than in the non-SE neurons. ***D***, Summary plots of early-sAHP amplitudes versus the number of spikes evoked by the depolarizing current pulses in the non-SE and post-SE neurons. Bar diagram represents the early-sAHP/Ns slopes in the two groups of neurons. The smaller early-sAHP/Ns slope in post-SE than in non-SE neurons implies that the early-sAHP is smaller in the former neurons. ***E***, Summary plots of late-sAHP amplitudes versus the number of spikes evoked by the depolarizing current pulses in the non-SE and post-SE neurons. Bar diagram represents the slow-sAHP/Ns slopes in the two groups of neurons. The two groups of neurons do not differ in late-sAHP amplitudes. ***F-J***, Same as in ***A-E***, but for non-SE ($n = 10$) and post-SE neurons ($n = 12$) in slices treated with 1 μM ATM. In this condition, the spike response gains and early-sAHP amplitudes in post-SE neurons resemble those of non-SE neurons. ***K-O***, Same as in ***A-E***, but for non-SE ($n = 11$) and post-SE neurons ($n = 12$) in slices treated with 1 μM NBI. In this condition also, the spike response gains and early-sAHP amplitudes in post-SE neurons resemble those of non-SE neurons. **$p < 0.01$. ***$p < 0.001$. NS, not significant

The firing responses and sAHPs evoked by 0.3 nA pulses in representative 1 μM ATM-treated non-SE and post-SE neurons are shown in Figure 8F, G. Under this treatment, the spike output gain of post-SE neurons was similar to that of non-SE neurons (49.8 ± 7.0 Ns/I, $n = 10$ vs 39.1 ± 5.7 Ns/I, $n = 12$, respectively; $p = 0.35$; Mann–Whitney test; Fig. 8H). Likewise, the early-sAHPs following the spike responses were also the same in post-SE compared with non-SE slices (0.27 ± 0.03 vs

0.24 ± 0.05 mV/Ns, respectively; $p = 0.77$; Mann–Whitney test; Fig. 8I), as were the late-sAHPs (0.06 ± 0.01 vs 0.05 ± 0.01 mV/Ns, respectively; $p = 0.2$; Mann–Whitney test; Fig. 8J).

The normalizing effects of ATM were mimicked by NBI. Representative recordings of the firing responses and sAHPs in 1 μM NBI-treated non-SE and post-SE neurons are shown in Figure 8K, L. Under this treatment, the spike output gain of post-SE neurons was similar to that of non-SE neurons

(49.9 ± 5.5 Ns/I, $n = 11$ vs 44.5 ± 2.2 Ns/I, $n = 12$, respectively; $p = 0.49$; Mann–Whitney test; Fig. 8M). Likewise, the early-sAHPs following the spike responses were also the same in post-SE versus non-SE slices (0.1 ± 0.01 vs 0.1 ± 0.01 mV/Ns, respectively; $p = 0.74$; Mann–Whitney test; Fig. 8N), as were the late-sAHPs (0.04 ± 0.01 vs 0.04 ± 0.004 mV/Ns, respectively; $p = 0.87$; Mann–Whitney test; Fig. 8O).

In summary, we found that $CRF_1R$ antagonism reduces the enhanced excitability of post-SE CA1 pyramidal cells, as expressed in their spike response gain, to that displayed by non-SE neurons. The normalization of excitability is because of the enhancement of the early-sAHPs consequent to removal of $CRF/CRF_1R/PKA$-induced $K_{Ca}3.1$ channel inhibition.

### ATM treatment reduces SRSs frequency in post-SE rats

The above results suggest that $CRF_1R$ antagonists may be effective in reducing seizure activity in post-SE rats. We tested the likelihood of this hypothesis in a pilot study using ATM, which, unlike NBI, did not affect $K_{Ca}$-sAHP/$I_{sAHP}$ amplitudes in non-SE rats (Fig. 5E). We used telemetric EEG analysis to automatically capture SRSs in post-SE rats intraperitoneally injected with the vehicle (DMSO) alone ($n = 6$ rats; Fig. 9A), or with the vehicle containing ATM ($n = 7$ rats; Fig. 9B). The frequencies of SRSs were monitored and quantified for 48 h, of which 24 h were before, and 24 h were after, injecting the rats. They are illustrated in the form of a "heat map" for each rat in Figure 9C. It is evident that the SRSs frequencies were quite variable throughout the recording period but were not markedly affected by vehicle injection (Rats 1-6). In contrast, SRSs frequencies were clearly reduced after ATM injection (Rats a-g). The mean numbers of SRSs for each consecutive hour during the 48 h recording period, normalized to the mean baseline SRSs frequency – the mean number of hourly SRSs appearing during the entire 24 h period before injection (mean $f_b$; Fig. 9D,E, dashed lines) are plotted for the vehicle- and ATM-injected rats in Figure 9D, E. These plots further highlight the decrease in SRSs frequency following ATM injection. The mean frequency of SRSs appearing during the 24 h period after injection (mean $f_a$; Fig. 9D,E, dotted lines) was not affected by the vehicle (from 1.00 ± 0.17 to 1.07 ± 0.14; $p = 0.791$; $n = 6$; Wilcoxon signed rank test; Fig. 9D, right), but was significantly reduced by ATM (from 1.00 ± 0.16 to 0.58 ± 0.12; $p = 0.027$; $n = 7$; Wilcoxon signed rank test; Fig. 9E, right), a 42% decrease. It is noteworthy that the mean hourly SRSs frequencies after ATM injection returned to the $f_b$ value for the first time only 21 h (Fig. 9E, hour 45). Thus, a single injection of ATM appears to exert an almost 24 h long anti-seizure effect.

Together, our results suggest that in pilocarpine-SE model, enhanced $CRF/CRF_1R/PKA$ signaling leads to downregulation of the $K_{Ca}$-sAHPs/$I_{sAHP}$s through PKA-dependent $K_{Ca}3.1$ inhibition, leading to intrinsic neuronal hyperexcitability. This alteration may contribute to the emergence of SRSs in post-SE rats, as $CRF_1R$ antagonism restores the $K_{Ca}$-sAHPs/$I_{sAHP}$s, normalizes intrinsic neuronal excitability, and reduces SRSs frequency.

## Discussion

Here we explored the epileptogenic mechanisms underlying the intrinsic hyperexcitability of post-SE CA1 pyramidal cells in an experimental model of acquired TLE. The data suggest that enhanced $CRF/CRF_1R/PKA$ signaling, possibly because of over-expression of $CRF/CRF_1R$ proteins, leads to sustained inhibition of $K_{Ca}3.1$ channels, manifested as $K_{Ca}$-sAHPs/$I_{sAHP}$s suppression

and increased spike response gain. Pharmacological antagonism of $CRF_1Rs$ reverses these cellular alterations and exerts an anti-seizure action in chronically epileptic post-SE rats. Together, these results suggest that $CRF/CRF_1R/PKA$-mediated $K_{Ca}3.1$ inhibition may play an important role in ictogenesis in experimental acquired TLE.

### $CRF_1Rs$ mediate inhibition of $K_{Ca}$-sAHPs/$I_{sAHP}$s

Previous studies have shown that CRF inhibits $K_{Ca}$-sAHPs/$I_{sAHP}$s in a PKA-dependent manner (Aldenhoff et al., 1983; Haug and Storm, 2000). Here we show further that this CRF action is mediated exclusively by $CRF_1Rs$. As both $CRF_1Rs$ and $CRF_2Rs$ can activate cAMP/PKA signaling pathways (Dautzenberg and Hauger, 2002), the unique involvement of $CRF_1Rs$ in $K_{Ca}$-sAHPs/$I_{sAHP}$s suppression likely reflects other features that distinguish them from $CRF_2Rs$, namely, their higher expression by hippocampal pyramidal cells (Chalmers et al., 1995; Chen et al., 2000; Van Pett et al., 2000; Tan et al., 2017), their larger affinity to CRF (Perrin et al., 1995), and/or their greater potency in stimulating cAMP production by adenylate cyclase (Grigoriadis et al., 1996).

Several neurotransmitters other than CRF were shown to suppress $K_{Ca}$-sAHPs/$I_{sAHP}$s through PKA activation on exogenous application (Madison and Nicoll, 1986; Pedarzani and Storm, 1993; Pedarzani et al., 1998; Haug and Storm, 2000). However, it is unlikely that one or more of these neurotransmitters is substantially upregulated in post-SE rats to cause $K_{Ca}$-sAHPs/$I_{sAHP}$s suppression, as $CRF_1R$ antagonism restored $K_{Ca}$-sAHPs/$I_{sAHP}$s almost completely to normal size.

The TRAM-34 sensitivity of $K_{Ca}$-sAHP/$I_{sAHP}$ restored in post-SE rats by $CRF_1R$ antagonists, as well as by PKA inhibitors (Tiwari et al., 2019), confirms that the overactive $CRF/CRF_1R/PKA$ signaling pathway in post-SE neurons targets $K_{Ca}3.1$ channels, highlighting their key role of these channels in maintaining normal brain excitability through $K_{Ca}$-sAHP/$I_{sAHP}$ generation.

### $CRF/CRF_1Rs$ upregulation in epileptogenesis

Our findings showing a remarkable increase (>200%) in both CRF and $CRF_1R$ protein expression in hippocampal tissue from post-SE rats, suggest that upregulation of hippocampal $CRF/CRF_1R$ neurotransmission may be a primary cause of enhanced $CRF/CRF_1R/PKA$ signaling, leading to $K_{Ca}$-sAHP/$I_{sAHP}$ downregulation and associated hyperexcitability of post-SE CA1 pyramidal cells.

An acute increase in CRF protein expression and in the number of CRF immunoreactive cells in the hippocampal formation was observed at 24 h following pilocarpine- and kainate-induced SE, but these observations were not extended to later time points (Piekut and Phipps, 1998, 1999; Wu et al., 2012). Interestingly, however, elevated expression of $CRF/CRF_1R$ was found in cortical tissues obtained posthumously from children with generalized epilepsy (Wang et al., 2001), as well as in cortical neurosurgical tissue obtained from children with intractable infantile spasms (Yang et al., 2017).

Further studies are required for localizing the cellular components displaying enhanced $CRF/CRF_1R$ protein expression in post-SE hippocampus and to identify the transcriptional factors involved in this process. A likely factor involved in epileptogenic CRF upregulation is the cytokine interleukin-6, a transcriptional activator of CRF (Navarra et al., 1991; Lyson and McCann, 1992; Vallières and Rivest, 1999; Kageyama et al., 2010), whose production and release markedly increase in the hippocampus during epileptogenesis as part of the aroused brain immune
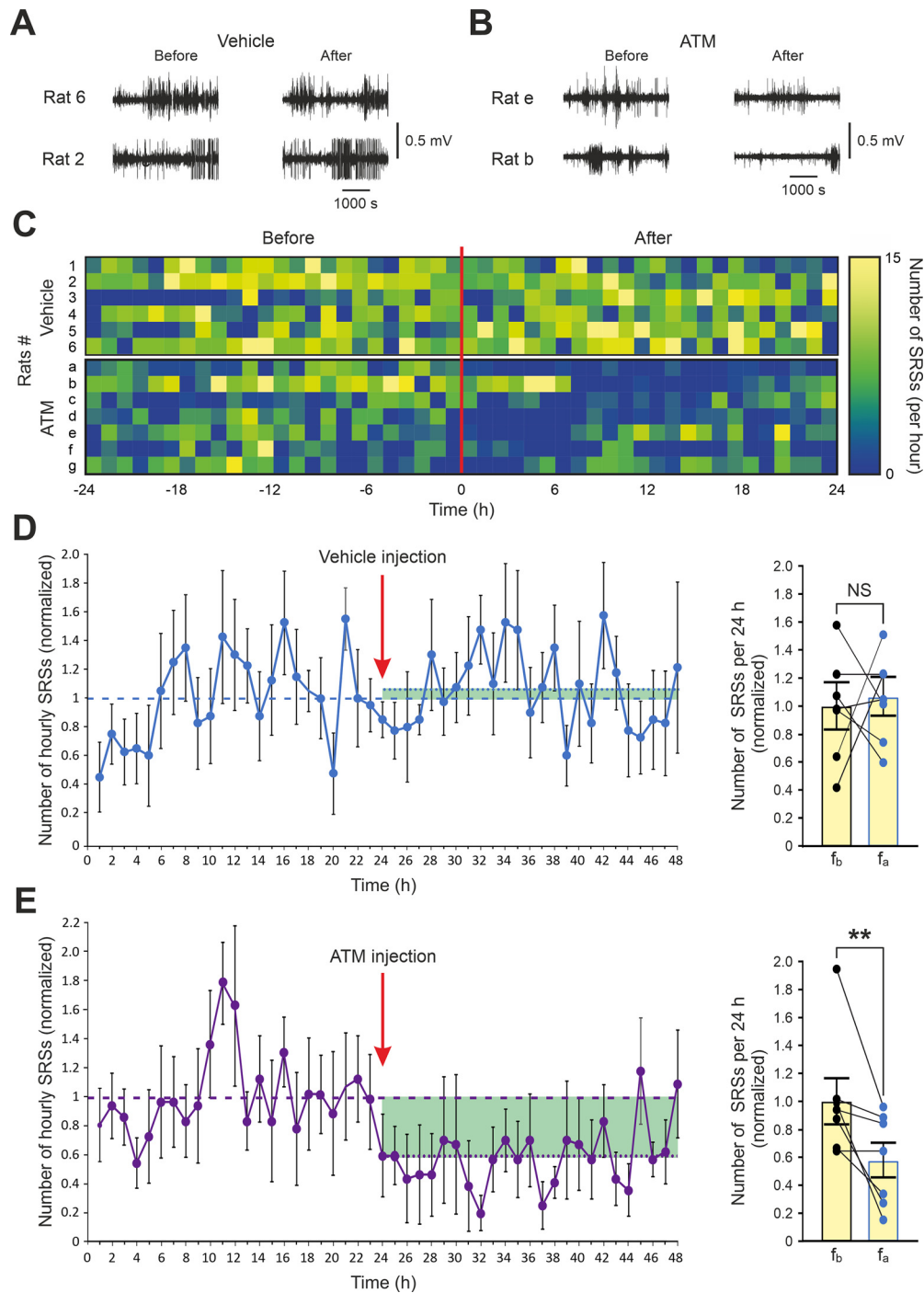
**Figure 9.** The CRF$_1$Rs antagonist ATM reduces SRSs frequency in post-SE rats. The SRSs were monitored in post-SE rats using continuous telemetric EEG recordings 24 h before and 24 h after injecting the vehicle alone (DMSO) or the vehicle containing ATM (20 mg/kg i.p.). *A*, Representative electrographic SRSs recoded before and after vehicle injection in 2 post-SE rats. *B*, Same as in *A*, but examples drawn from ATM-injected post-SE rats. *C*, A heat map describing the frequency per hour of SRSs during each of the 48 h of recording for each rat injected either with the vehicle (Rats 1-6) or with ATM (Rats a-g). It is evident that all and only ATM-injected rats display a reduction in SRSs frequency lasting several hours after injection. *D*, Left, Summary plot displaying the average SRSs frequencies in the 6 vehicle-injected rats throughout the 48-h-long recording period. Arrow indicates the time of injection. Each point represents the average frequency of SRSs detected during a bin of 1 h, normalized to the average hourly frequency of SRSs detected in all rats during the 24 h before injection (mean f$_b$; dashed line). Also depicted is the average hourly frequency of SRSs detected in all rats during the 24 h after injection (mean f$_a$; dotted line). Right, Summary bar diagram showing the f$_b$ and f$_a$ values for each rat. The mean f$_b$ and f$_a$ do not differ significantly. *E*, Same as in *D*, but for the 7 ATM-injected rats. The mean f$_a$ is significantly small than the mean f$_b$. **$p < 0.01$. NS, not significant.

response (De Simoni et al., 2000; Lehtimäki et al., 2003; Chmielewska et al., 2021).

**Translational implications**

The successful normalization of intrinsic excitability of post-SE neurons by CRF$_1$R antagonists prompted us to test

whether this pharmacological intervention may exert an anti-seizure action in post-SE rats *in vivo*. We found that a single dose of intraperitoneally injected ATM significantly reduced the 24 h average SRSs frequency by 41%, whereas a similar injection of the vehicle had no significant effect on this frequency. Interestingly, an anti-seizure effect of

CRF$_1$R antagonists was recently found also in EEG recordings from amygdala of rats subjected to traumatic brain injury, another type of insult causing TLE (Narla et al., 2019).

It is tempting to assume that the anti-seizure action of ATM is mediated primarily by restoration of K$_{Ca}$3.1 channel activity. Yet, other consequences of CRF$_1$Rs antagonism may contribute in part to this action. In particular, ATM was shown to interfere with the brain's stress response by blocking CRF/CRF$_1$R-induced ACTH release from the anterior pituitary gland (Webster et al., 1996). It is generally thought that stress and seizures mutually enhance one another (Maguire and Salpekar, 2013). However, there is no evidence that stress modulates the frequency of SRSs in post-SE rats. Indeed, corticosterone injection into pilocarpine post-SE mice did not alter the frequency of electrographic SRSs (Castro et al., 2012). Intriguingly, corticosterone application to ordinary CA1 pyramidal cells even enhanced the sAHPs and reduced spike output (Joëls and De Kloet, 1989), an action opposite to that of CRF. Therefore, it is doubtful that interaction with the hypothalamic-pituitary-adrenal axis contributes significantly to the anti-seizure action of ATM described in the present study. Further studies are required to characterize the involvement of the hypothalamic-pituitary-adrenal axis in ATM's anti-seizure action (Basu et al., 2021).

In conclusion, our study identified enhanced CRF/CRF$_1$R/PKA signaling as a key mechanism underlying the hyperexcitability of principal hippocampal neurons, which may be causally related to SRSs generation in experimental acquired TLE. Therefore, we suggest that ATM, or other orally bioavailable CRF$_1$R antagonists, should be tested further as anti-seizure therapy in experimental and in human acquired epilepsy. Given that the anti-seizure effect of a single ATM injection lasted for 21 h, it is likely that a daily administration of this drug may turn out to be a satisfactory therapeutic regimen. To that end, it is encouraging to note that in clinical studies of CRF$_1$R antagonists as remedies for depression and anxiety, the drugs lacked significant adverse side effects (Künzel et al., 2003; Binneman et al., 2008; Coric et al., 2010).

## References

Aldenhoff JB, Gruol DL, Rivier J, Vale W, Siggins GR (1983) Corticotropin releasing factor decreases postburst hyperpolarizations and excites hippocampal neurons. Science 221:875–877.

Azouz R, Jensen MS, Yaari Y (1994) Muscarinic modulation of intrinsic burst firing in rat hippocampal neurons. Eur J Neurosci 6:961–966.

Baram TZ, Schultz L (1991) Corticotropin-releasing hormone is a rapid and potent convulsant in the infant rat. Brain Res Dev Brain Res 61:97–101.

Basu T, Maguire J, Salpekar JA (2021) Hypothalamic-pituitary-adrenal axis targets for the treatment of epilepsy. Neurosci Lett 746:135618.

Becker AJ (2018) Review: animal models of acquired epilepsy: insights into mechanisms of human epileptogenesis. Neuropathol Appl Neurobiol 44:112–129.

Binneman B, Feltner D, Kolluri S, Shi Y, Qiu R, Stiger T (2008) A 6-week randomized, placebo-controlled trial of CP-316,311 (a selective CRH1 antagonist) in the treatment of major depression. Am J Psychiatry 165:617–620.

Brunson KL, Eghbal-Ahmadi M, Baram TZ (2001) How do the many etiologies of West syndrome lead to excitability and seizures? The corticotropin releasing hormone excess hypothesis. Brain Dev 23:533–538.

Castro OW, Santos VR, Pun RY, McKlveen JM, Batie M, Holland KD, Gardner M, Garcia-Cairasco N, Herman JP, Danzer SC (2012) Impact of corticosterone treatment on spontaneous seizure frequency and epileptiform activity in mice with chronic epilepsy. PLoS One 7:e46044.

Chalmers DT, Lovenberg TW, De Souza EB (1995) Localization of novel corticotropin-releasing factor receptor (CRF2) mRNA expression to specific subcortical nuclei in rat brain: comparison with CRF1 receptor mRNA expression. J Neurosci 15:6340–6350.

Chen C, Dagnino R, De Souza EB, Grigoriadis DE, Huang CQ, Kim KI, Liu Z, Moran T, Webb TR, Whitten JP, Xie YF, McCarthy JR Jr (1996) Design and synthesis of a series of non-peptide high-affinity human corticotropin-releasing factor1 receptor antagonists. J Med Chem 39:4358–4360.

Chen Y, Brunson KL, Müller MB, Cariaga W, Baram TZ (2000) Immunocytochemical distribution of corticotropin-releasing hormone receptor type-1 (CRF1)-like immunoreactivity in the mouse brain: light microscopy analysis using an antibody directed against the c-terminus. J Comp Neurol 420:305–323.

Chen Y, Brunson KL, Adelmann G, Bender RA, Frotscher M, Baram TZ (2004) Hippocampal corticotropin releasing hormone: pre- and postsynaptic location and release by stress. Neuroscience 126:533–540.

Chijiwa T, Mishima A, Hagiwara M, Sano M, Hayashi K, Inoue T, Naito K, Toshioka T, Hidaka H (1990) Inhibition of forskolin-induced neurite outgrowth and protein phosphorylation by a newly synthesized selective inhibitor of cyclic AMP-dependent protein kinase, N-[2-(p-bromocinnamylamino)ethyl]-5-isoquinolinesulfonamide (H-89), of pc12d pheochromocytoma. J Biol Chem 265:5267–5272.

Chmielewska N, Maciejak P, Osuch B, Kursa MB, Szyndler J (2021) Pro-inflammatory cytokines, but not brain- and extracellular matrix-derived proteins, are increased in the plasma following electrically induced kindling of seizures. Pharmacol Rep 73:506–515.

Coric V, Feldman HH, Oren DA, Shekhar A, Pultz J, Dockens RC, Wu X, Gentile KA, Huang SP, Emison E, Delmonte T, D'Souza BB, Zimbroff DL, Grebb JA, Goddard AW, Stock EG (2010) Multicenter, randomized, double-blind, active comparator and placebo-controlled trial of a corticotropin-releasing factor receptor-1 antagonist in generalized anxiety disorder. Depress Anxiety 27:417–425.

Dautzenberg FM, Hauger RL (2002) The CRF peptide family and their receptors: yet more partners discovered. Trends Pharmacol Sci 23:71–77.

De Simoni MG, Perego C, Ravizza T, Moneta D, Conti M, Marchesi F, De Luigi A, Garattini S, Vezzani A (2000) Inflammatory cytokines and related genes are induced in the rat hippocampus by limbic status epilepticus. Eur J Neurosci 12:2623–2633.

Delaware M, Tezuka T, Kiyama Y, Yokoyama K, Inoue T, Hattori S, Hashimoto R, Umemori H, Manabe T, Yamamoto T, Nakazawa T (2010) NMDAR2b tyrosine phosphorylation regulates anxiety-like behavior and CRF expression in the amygdala. Mol Brain 3:37.

Ehlers CL, Henriksen SJ, Wang M, Rivier J, Vale W, Bloom FE (1983) Corticotropin releasing factor produces increases in brain excitability and convulsive seizures in rats. Brain Res 278:332–336.

Fortes PM, Albrechet-Souza L, Vasconcelos M, Ascoli BM, Menegolla AP, de Almeida RM (2017) Instigação social e confrontos agressivos repetidos em camundongos Swiss machos: análise de corticosterona plasmática e dos níveis de CRF e BDNF em áreas cerebrais límbicas. Trends Psychiatry Psychother 39:98–105.

Gai Z, Li K, Sun H, She X, Cui B, Wang R (2016) Effects of chronic noise on mRNA and protein expression of CRF family molecules and its relationship with p-tau in the rat prefrontal cortex. J Neurol Sci 368:307–313.

Grigoriadis DE, Lovenberg TW, Chalmers DT, Liaw C, De Souza EB (1996) Characterization of corticotropin-releasing factor receptor subtypes. Ann NY Acad Sci 780:60–80.

Gulledge AT, Dasari S, Onoue K, Stephens EK, Hasse JM, Avesar D (2013) A sodium-pump-mediated afterhyperpolarization in pyramidal neurons. J Neurosci 33:13025–13041.

Gunn BG, Sanchez GA, Lynch G, Baram TZ, Chen Y (2019) Hyper-diversity of CRH interneurons in mouse hippocampus. Brain Struct Funct 224:583–598.

Habib KE, Weld KP, Rice KC, Pushkas J, Champoux M, Listwak S, Webster EL, Atkinson AJ, Schulkin J, Contoreggi C, Chrousos GP, McCann JS, Suomi SJ, Higley JD, Gold PW (2000) Oral administration of a corticotropin-releasing hormone receptor antagonist significantly attenuates behavioral, neuroendocrine, and autonomic responses to stress in primates. Proc Natl Acad Sci USA 97:6079–6084.

Haug T, Storm JF (2000) Protein kinase A mediates the modulation of the slow $Ca^{2+}$-dependent $K^+$ current, $I_{sAHP}$, by the neuropeptides CRF, VIP, and CGRP in hippocampal pyramidal neurons. J Neurophysiol 83:2071–2079.

Jensen MS, Azouz R, Yaari Y (1996) Spike after-depolarization and burst generation in adult rat hippocampal CA1 pyramidal cells. J Physiol 492:199–210.

Joëls M, De Kloet ER (1989) Effects of glucocorticoids and norepinephrine on the excitability in the hippocampus. Science 245:1502–1505.

Kageyama K, Kagaya S, Takayasu S, Hanada K, Iwasaki Y, Suda T (2010) Cytokines induce NF-$\kappa$B, Nurr1 and corticotropin-releasing factor gene transcription in Hypothalamic 4B cells. Neuroimmunomodulation 17:305–313.

King B, Rizwan AP, Asmara H, Heath NC, Engbers JD, Dykstra S, Bartoletti TM, Hameed S, Zamponi GW, Turner RW (2015) $IK_{Ca}$ channels are a critical determinant of the slow AHP in CA1 pyramidal neurons. Cell Rep 11:175–182.

Künzel HE, Zobel AW, Nickel T, Ackl N, Uhr M, Sonntag A, Ising M, Holsboer F (2003) Treatment of depression with the CRH-1-receptor antagonist R121919: endocrine changes and side effects. J Psychiatr Res 365:919–926.

Kwan P, Schachter SC, Brodie MJ (2011) Drug-resistant epilepsy. N Engl J Med 365:919–926.

Lehtimäki KA, Peltola J, Koskikallio E, Keränen T, Honkaniemi J (2003) Expression of cytokines and cytokine receptors in the rat brain after kainic acid-induced seizures. Brain Res Mol Brain Res 110:253–260.

Lovenberg TW, Liaw CW, Grigoriadis DE, Clevenger W, Chalmers DT, De Souza EB, Oltersdorf T (1995) Cloning and characterization of a functionally distinct corticotropin-releasing factor receptor subtype from rat brain. Proc Natl Acad Sci USA 92:836–840.

Lyson K, McCann SM (1992) Involvement of arachidonic acid cascade pathways in lnterleukin-6-stimulated corticotropin-releasing factor release in vitro. Neuroendocrinology 55:708–713.

Madison DV, Nicoll RA (1986) Cyclic adenosine 3',5'-monophosphate mediates beta-receptor actions of noradrenaline in rat hippocampal pyramidal cells. J Physiol 372:245–259.

Maguire J, Salpekar JA (2013) Stress, seizures, and hypothalamic-pituitary-adrenal axis targets for the treatment of epilepsy. Epilepsy Behav 26:352–362.

Mohan S, Tiwari MN, Biala Y, Yaari Y (2019) Regulation of neuronal Na+/K+-ATPase by specific protein kinases and protein phosphatases. J Neurosci 39:5440–5451.

Mohan S, Tiwari MN, Stanojević M, Biala Y, Yaari Y (2021) Muscarinic regulation of the neuronal $Na^+/K^+$-ATPase in rat hippocampus. J Physiol 599:3735–3754.

Narla C, Jung PS, Bautista Cruz F, Everest M, Martinez-Trujillo J, Poulter MO (2019) CRF mediates stress-induced pathophysiological high-frequency oscillations in traumatic brain injury. eNeuro 6:ENEURO.0334-18.2019.

Navarra P, Tsagarakis S, Faria MS, Rees LH, Besser GM, Grossman AB (1991) Interleukins-1 and -6 stimulate the release of corticotropin-releasing hormone-41 from rat hypothalamus in vitro via the eicosanoid cyclo-oxygenase pathway. Endocrinology 128:37–44.

Pedarzani P, Krause M, Haug T, Storm JF, Stühmer W (1998) Modulation of the $Ca^{2+}$-activated $K^+$ current sI(AHP) by a phosphatase-kinase balance under basal conditions in rat CA1 pyramidal neurons. J Neurophysiol 79:3252–3256.

Pedarzani P, Storm JF (1993) PKA mediates the effects of monoamine transmitters on the $K^+$ current underlying the slow spike frequency adaptation in hippocampal neurons. Neuron 11:1023–1035.

Perrin M, Donaldson C, Chen R, Blount A, Berggren T, Bilezikjian L, Sawchenko P, Vale W (1995) Identification of a second corticotropin-releasing factor receptor gene and characterization of a cDNA expressed in heart. Proc Natl Acad Sci USA 92:2969–2973.

Perrin MH, Vale WW (1999) Corticotropin releasing factor receptors and their ligand family. Ann NY Acad Sci 885:312–328.

Piekut DT, Phipps B (1998) Increased corticotropin-releasing factor immunoreactivity in select brain sites following kainate-elicited seizures. Brain Res 781:100–113.

Piekut DT, Phipps B (1999) Corticotropin-releasing factor: immunolabeled fibers in brain regions with localized kainate neurotoxicity. Acta Neuropathol 98:622–628.

Raol YH, Brooks-Kayal AR (2012) Experimental models of seizures and epilepsies. Prog Mol Biol Transl Sci 105:57–82.

Rivier J, Gulyas J, Kirby D, Low W, Perrin MH, Kunitake K, DiGruccio M, Vaughan J, Reubi JC, Waser B, Koerber SC, Martinez V, Wang L, Taché Y, Vale W (2002) Potent and long-acting corticotropin releasing factor (CRF) receptor 2 selective peptide competitive antagonists. J Med Chem 45:4737–4747.

Roshchin MV, Ierusalimsky VN, Balaban PM, Nikitin ES (2020) $Ca^{2+}$-activated $K_{Ca}$3.1 potassium channels contribute to the slow afterhyperpolarization in L5 neocortical pyramidal neurons. Sci Rep 10:14484.

Sahu G, Wazen RM, Colarusso P, Chen SR, Zamponi GW, Turner RW (2019) Junctophilin proteins tether a Cav1-RyR2-$K_{Ca}$3.1 tripartite complex to regulate neuronal excitability. Cell Rep 28:2427–2442. e6.

Sahu G, Turner RW (2021) The molecular basis for the calcium-dependent slow afterhyperpolarization in CA1 hippocampal pyramidal neurons. Front Physiol 12:759707.

Sanabria ER, Su H, Yaari Y (2001) Initiation of network bursts by $Ca^{2+}$-dependent intrinsic bursting in the rat pilocarpine model of temporal lobe epilepsy. J Physiol 532:205–216.

Sick J, Bray E, Bregy A, Dietrich WD, Bramlett HM, Sick T (2013) EEGgui: a program used to detect electroencephalogram anomalies after traumatic brain injury. Source Code Biol Med 8:12.

Tamir I, Daninos M, Yaari Y (2017) Plasticity of intrinsic firing response gain in principal hippocampal neurons following pilocarpine-induced status epilepticus. Neuroscience 357:325–337.

Tan LA, Vaughan JM, Perrin MH, Rivier JE, Sawchenko PE (2017) Distribution of corticotropin-releasing factor (CRF) receptor binding in the mouse brain using a new, high-affinity radioligand, [125I]-PD-Sauvagine. J Comp Neurol 525:3840–3864.

Téllez-Zenteno JF, Hernández-Ronquillo L (2012) A review of the epidemiology of temporal lobe epilepsy. Epilepsy Res Treat 2012:630853–630855.

Tiwari MN, Singh AK, Ahmad I, Upadhyay G, Singh D, Patel DK, Singh C, Prakash O, Singh MP (2010) Effects of cypermethrin on monoamine transporters, xenobiotic metabolizing enzymes and lipid peroxidation in the rat nigrostriatal system. Free Radic Res 44:1416–1424.

Tiwari MN, Mohan S, Biala Y, Yaari Y (2018) Differential contributions of $Ca^{2+}$-activated $K^+$ channels and $Na^+/K^+$-ATPases to the generation of the slow afterhyperpolarization in CA1 pyramidal cells. Hippocampus 28:338–357.

Tiwari MN, Mohan S, Biala Y, Yaari Y (2019) Protein kinase A-mediated suppression of the slow afterhyperpolarizing KCa3.1 current in temporal lobe epilepsy. J Neurosci 39:9914–9926.

Turner RW, Kruskic M, Teves M, Scheidl-Yee T, Hameed S, Zamponi GW (2015) Neuronal expression of the intermediate conductance calcium-activated potassium channel KCa3.1 in the mammalian central nervous system. Pflugers Arch Eur Arch 467:311–328.

Turner RW, Asmara H, Engbers JD, Miclat J, Rizwan AP, Sahu G, Zamponi GW (2016) Assessing the role of $IK_{Ca}$ channels in generating the sAHP of CA1 hippocampal pyramidal cells. Channels (Austin) 10:313–319.

Turski WA, Cavalheiro EA, Schwarz M, Czuczwar SJ, Kleinrok Z, Turski L (1983) Limbic seizures produced by pilocarpine in rats: behavioural, electroencephalographic and neuropathological study. Behav Brain Res 9:315–335.

Vallières L, Rivest S (1999) Interleukin-6 is a needed proinflammatory cytokine in the prolonged neural activity and transcriptional activation of corticotropin-releasing factor during endotoxemia. Endocrinology 140:3890–3903.

Van Pett K, Viau V, Bittencourt JC, Chan RK, Li HY, Arias C, Prins GS, Perrin M, Vale W, Sawchenko PE (2000) Distribution of mRNAs encoding CRF receptors in brain and pituitary of rat and mouse. J Comp Neurol 428:191–212.

Velumian AA, Zhang L, Pennefather P, Carlen PL (1997) Reversible inhibition of $I_K$, $I_{AHP}$, $I_h$ and $I_{Ca}$ currents by internally applied gluconate in rat hippocampal pyramidal neurons. Pflugers Arch Eur Arch 433:343–350.

Wahab A (2010) Difficulties in treatment and management of epilepsy and challenges in new drug development. Pharmaceuticals (Basel) 3:2090–2110.

Wang W, Dow KE, Fraser DD (2001) Elevated corticotropin releasing hormone/corticotropin releasing hormone-R1 expression in postmortem brain obtained from children with generalized epilepsy. Ann Neurol 50:404–409.

Webster EL, Lewis DB, Torpy DJ, Zachman EK, Rice KC, Chrousos GP (1996) In vivo and in vitro characterization of antalarmin, a nonpeptide corticotropin-releasing hormone (CRH) receptor antagonist: suppression of pituitary ACTH release and peripheral inflammation. Endocrinology 137:5747–5750.

Wu J, Ma DL, Ling EA, Tang FR (2012) Corticotropin releasing factor (CRF) in the hippocampus of the mouse pilocarpine model of status epilepticus. Neurosci Lett 512:83–88.

Wulff H, Miller MJ, Hänsel W, Grissmer S, Cahalan MD, Chandy KG (2000) Design of a potent and selective inhibitor of the intermediate-conductance $Ca^{2+}$-activated $K^+$ channel, IKCa1: a potential immunosuppressant. Proc Natl Acad Sci USA 97:8151–8156.

Yang XL, Chen B, Zhang XQ, Chen X, Yang MH, Zhang W, Chen HR, Zang ZL, Li W, Yang H, Liu SY (2017) Upregulations of CRH and CRHR1 in the epileptogenic tissues of patients with intractable infantile spasms. CNS Neurosci Ther 23:57–68.

Zhang J, Zhang C, Chen X, Wang B, Ma W, Yang Y, Zheng R, Huang Z (2021) PKA-RII$\beta$ autophosphorylation modulates PKA activity and seizure phenotypes in mice. Commun Biol 4:263.